

SECTION II. TASK 2. SUBMODEL DEVELOPMENT AND EVALUATION

Objectives

The objectives of this task are to develop or adapt advanced physics and chemistry submodels for the reactions of coal in an entrained-bed and a fixed-bed reactor and to validate the submodels by comparison with laboratory scale experiments.

Task Outline

The development of advanced submodels for the entrained-bed and fixed-bed reactor models will be organized into the following categories: a) Coal Chemistry (including coal pyrolysis chemistry, char formation, particle mass transfer, particle thermal properties, and particle physical behavior); b) Char Reaction Chemistry at high pressure; c) Secondary Reactions of Pyrolysis Products (including gas-phase cracking, soot formation, ignition, char burnout, sulfur capture, and tar/gas reactions); d) Ash Physics and Chemistry (including mineral characterization, evolution of volatile, molten and dry particle components, and ash fusion behavior); e) Large Coal Particle Effects (including temperature, composition, and pressure gradients and secondary reactions within the particle, and the physical affects of melting, agglomeration, bubble formation and bubble transport; f) Large Char Particle Effects (including oxidation); g) SO_x - NO_x Submodel Development (including the evolution and oxidation of sulfur and nitrogen species); and h) SO_x and NO_x Model Evaluation.

II.A. SUBTASK 2.a. - COAL TO CHAR CHEMISTRY SUBMODEL DEVELOPMENT AND EVALUATION

Senior Investigator - David G. Hamblen
Advanced Fuel Research, Inc.
87 Church Street, East Hartford, CT 06108
(203) 528-9806

Objective

The objective of this subtask is to develop and evaluate, by comparison with laboratory experiments, an integrated and compatible submodel to describe the organic chemistry and physical changes occurring during the transformation from coal to char in coal conversion processes. Many of the data and some computer codes for this submodel are available, so it is expected that a complete integrated code will be developed during Phase I. Improvements in accuracy and efficiency will be pursued during Phase II.

Accomplishments

Additional improvements were made in the FG-DVC model. A second version of the model was developed for reactors in which the tar is quenched after being evolved. The model run procedure was modified so that successive cases could be run in a batch mode and the results could be averaged, stored and/or plotted. The creation and loss of methyl groups in the DVC model due to bridge breaking and in the FG model due to methane formation was made consistent. In addition, improvements were made in the way that crosslinking is treated in the model.

The FG-DVC model was used to predict baseline pyrolysis data for the eight Argonne coals from three different reactors. In general, the model did a good job in predicting the data for gas, tar and char yields and for the tar molecular weight distributions.

In order to refine the combined kinetic/mass transport submodel used in the FG-DVC model, a search was made of literature pyrolysis data for the Pittsburgh Seam coal, starting with heated grid experiments. When a comparison was made of data produced by heating at 1000 K/s to various peak temperatures, it was found that the results of different investigators did not agree, even when obtained from the same laboratory. We begin an experimental and theoretical study into possible reasons for these variations, which we are doing in conjunction with Professor Eric Suuberg of Brown University.

Modeling

The modeling work included: a) making improvements to the FG-DVC model and b) using the model to simulate the baseline pyrolysis experiments. This work is described below:

Model Improvements

A second version of the FG-DVC model was developed for reactors in which the tar is quenched after being evolved, such as in a heated grid reactor. This version is being used for the simulations of the TG/FTIR and FIMS experiments, while the previous version is used in the simulations for the entrained flow reactor (EFR), in which the tar continues to react to form light gases after being evolved. In addition, the run procedure was modified for both versions so that successive cases could be run in a batch mode and the results stored and/or plotted, without operator intervention.

The plotting program was also modified so that direct comparisons could be made to the data produced from a series of experiments in the entrained flow reactor. The models to describe gas phase cracking of hydrocarbon volatiles and equilibrium of CH_4 , H_2O , CO , H_2 and CO_2 , which were developed under previous DOE projects to work with the FG model, will be added to the FG-DVC model. During the past quarter, these models were transferred to the SUN computer where the FG/DVC program resides.

The creation and loss of methyl groups in the DVC model due to bridge breaking and in the FG model due to methane formation was made consistent so that both parts of the model are in agreement. In addition, further improvements were made in regard to the crosslinking coefficients for CO_2 and CH_4 . Previously, the crosslinking coefficients for CO_2 and CH_4 were chosen to be 1.0 and 0.75, respectively, based on the amount of each gas species evolved from both the char and tar. Since the CO_2 and CH_4 evolved from tar make no contribution to crosslinking, the modified code now takes the crosslinking coefficients of both CO_2 and CH_4 as unity and only counts the part of the these gases formed from char as being responsible for crosslinking in the char.

Due to the statistical nature of the Monte Carlo method, the tar molecular

weight distributions predicted by individual runs of the FG-DVC simulation often show a noticeable fluctuation. To eliminate the statistical fluctuations, the FG-DVC code has been modified so that the code can be run continuously for as many times as designated without interruption and the tar molecular weight distributions are automatically summed up and averaged over these runs. A comparison of an individual simulation with an averaged set of simulations is shown in Fig. II.A-1. The averaged spectrum is much smoother.

Model Applications

The FG-DVC model was used to model baseline pyrolysis data for the eight Argonne coals from three reactors (entrained flow reactor (EFR), TG-FTIR, and Field Ionization Mass Spectrometry (FIMS)). Elemental and ultimate analysis data are given for the eight Argonne coals in Table II.A-1. In general, the FG-DVC model did a good job in predicting the data for gas and tar yields and in predicting the shapes of the tar molecular weight distributions obtained by FIMS. The only species that was not well predicted was water, where the data are widely scattered. This work is summarized below.

Experimental Data

The experimental results for these coals from the TG-FTIR apparatus have been presented in the Sixth quarterly report. These data showed some variations (e.g., 15°C for CH₄, 60°C for tar, 60-90°C for most oxygenates) in the peak temperatures for the maximum evolution rate, particularly in the case of oxygenated volatiles. The variations in the peak temperatures for the various species are consistent with results from an earlier programmed pyrolysis experiment on ten coals (Solomon and Hamblen, 1983). However, for each species, the variation in the peak temperature with rank is small relative to a) the width of the peak; b) the variations among species; c) the variations among experiments with significantly different heating rates; d) the typical variations in the data of different investigators for the same species from the same coal. In view of the relative insensitivity of individual species kinetics when compared to these factors, the FG-DVC model assumption of rank independent rates appears sound. The corollary conclusion that the principal variation of pyrolysis behavior with rank is due to variations in the concentration of functional groups and hence, the amount of each pyrolysis product is also unchanged. These conclusions are supported by the ability of the FG-DVC model, which incorporates these assumptions, to fit pyrolysis data for a wide range of coal types over a wide range of conditions, as discussed below.

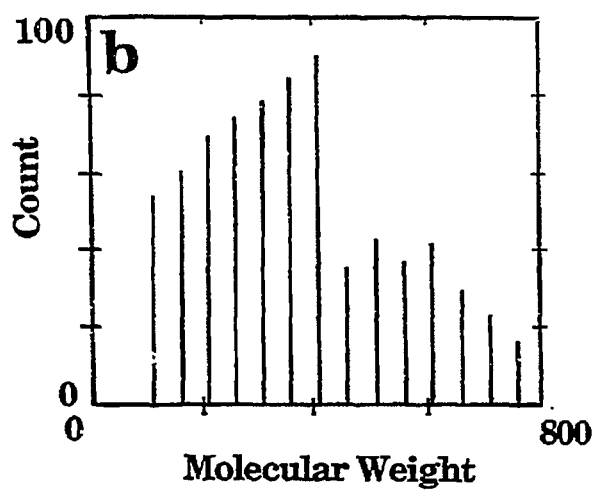
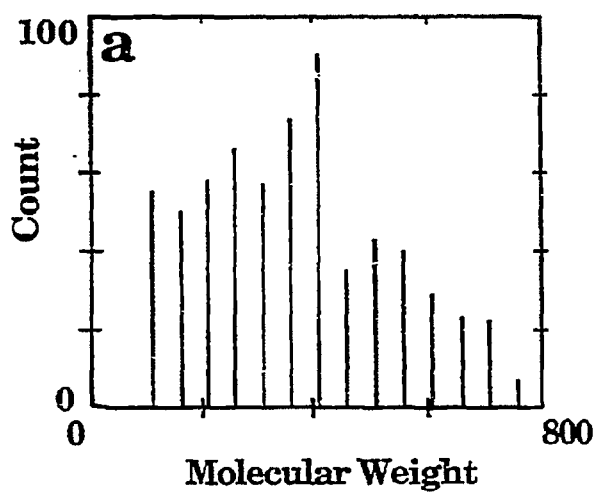


Figure 11A-1. Comparison of Simulation of FIMS Data for (a) Single FG-DVC Run to (b) an Average of Several Runs.

Table IIA-1 -Elemental Analysis of Argonne Premium Coal Samples.

	% daf Basis					As-Received	
	C	H	O	N	S	% Dry Basis	Basis
						Ash	Moisture
1. Pocahontas	90	4.7	8	1.3	1.0	5	0.6
2. Upper Freeport	84	5.0	7	1.5	2.5	13	1.1
3. Pittsburgh #8	82	5.8	8.8	1.6	1.8	9	1.6
4. Lewiston-Stockton	81	5.5	11	1.6	0.8	20	2.4
5. Utah Blind Canyon	79	6.0	13	1.6	0.5	5	4.6
6. Illinois #6	76	5.7	10	1.4	6.4	16	8.0
7. Wyodak	74	5.1	19	1.1	0.4	8	28.1
8. Beulah-Zap	72	5.2	21	1.1	0.8	6	32.2

The data for the EFR experiments has been given in the First Annual Report. Only the data for the 700°C and 1100°C experiments has been modeled so far. All of the coals show the influence of secondary cracking reactions above 700°C and secondary gasification reactions above 1100°C. At 1400°C, the products are close to thermodynamic equilibrium in both cases and consist primarily of char, CO, and H₂. Models have been developed to describe secondary reactions (Serio et al., 1987), but these have not been included in the version of the model used here, except for the tar cracking which is part of the standard FG model used for reactors where the tar is not quenched (Solomon, et al., 1988; Serio et al., 1987). Consequently, we do not show model predictions for the 1400°C EFR experiments which are dominated by these effects.

Determination of Parameters for the FG-DVC Model

The FG-DVC model contains several parameters, some of which depend on the coal and one which depends on the experiment type. The large number of parameters has been criticized by some. However, it should be pointed out that the model is able to predict a large number of pyrolysis phenomena such as the yields of individual gas species, the yields of tar and char, the tar molecular weight distribution, the crosslink density and the viscosity. The model also accounts for the variation of these quantities with temperature, heating rate, residence time, and pressure in a manner that agrees well with experiment. The details of the model inputs and a sensitivity analysis are included in a recent paper (Solomon, 1988).

The first step is to obtain elemental analysis data for C,H,N,O, and S. This is needed to construct a coal composition file. The next step is to determine the amounts of the individual functional group (FG) pools (CO₂-extra loose, CO₂-loose, CO₂-tight, CH₄-loose, etc). This requires data from at least two standard pyrolysis experiments. The first is a slow heating pyrolysis experiment, like the TG-FTIR experiment, which can provide good quantitative gas yields and differential evolution curves. This type of experiment is best able to resolve the individual loose, tight, etc. pools for a given gas, especially when both the integral and differential curves are compared with the model predictions. The values of the FG pools so determined are checked against a second pyrolysis experiment done at high heating rates, such as the EFR 1100°C data. The pools are adjusted to simultaneously fit the low and high heating rate experiments. This usually involves a series of iterations.

This procedure has been followed for the eight Argonne coals and the results

are shown in Fig. II.A-2 for the major FG pools, which are CH₄, CO₂, H₂O, and CO. These values have not yet been fully optimized and may change slightly in the future, but give good agreement with experiment, except in the case of H₂O where the data are scattered. The oxygenated species show a systematic increase with decreasing rank. The amount of CH₄ goes through a maximum in the medium rank coals, as do other hydrocarbon species such as tar (see below).

Once the functional group pools have been established to allow a good match between the integral and/or differential yield curves for two pyrolysis experiments, the input parameters for the DVC (tar formation) part of the model are determined. The first step is to adjust the average oligomer length to match the coal extract yield. The next step is to adjust the number of unbreakable bridges ("hard" bonds) between monomer clusters to fit the experimentally observed tar yields for the same low and high heating rate experiments used to calibrate the functional group pools. The relationships between these input quantities and the experimentally measured quantities are shown in Figs. II.A-3 and II.A-4. The extract yield data (which were obtained from Professor Milton Lee at Brigham Young University) and the average oligomer length are inversely correlated. The same is true of the number of hard bonds and the tar yield. Again, these values have not been fully optimized and are subject to change.

Other parameters which go into the tar formation model are the average monomer molecular weight (M_{avg}) and the average molecular weight between crosslinks (M_c). The value of M_c is interpolated from the literature data of Nelson (1983). We eventually plan to use literature data for M_{avg} as well. However, the size of the average cluster varies significantly among different research groups and the reported rank variations are not systematic or clearly understood. Currently, we are using a value of 256 for all the coals except the Pocahontas where a value of 506 is used. The significantly higher average cluster size for the Pocahontas compared to the others is supported by the calculations of Gerstein et al. (1982) based on NMR, FT-IR and elemental analysis data obtained for a number of coals.

The last important parameter to be selected is the value of ΔP , which is the average pressure difference between the ambient and the particle's interior during pyrolysis. This parameter is used in the internal transport model. The choice of ΔP has a significant effect on tar yield and the tar molecular weight distribution for non-softening coals under most conditions except high pressure. For fluid coals, a value of $\Delta P = 0$ is a good approximation for pressures of one atm or

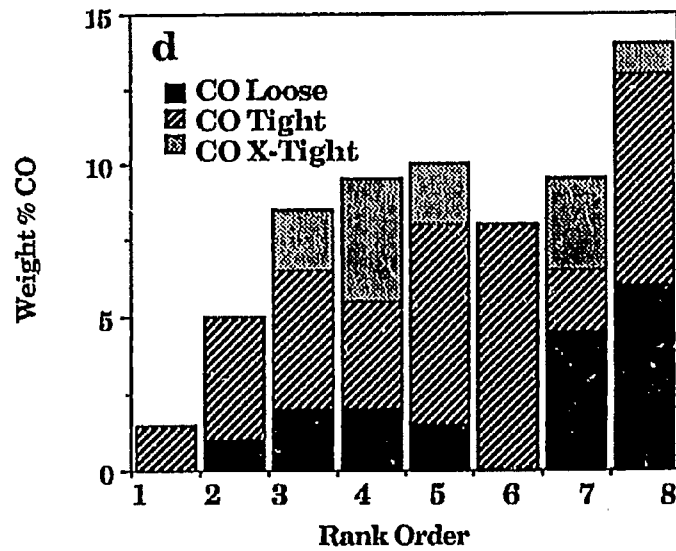
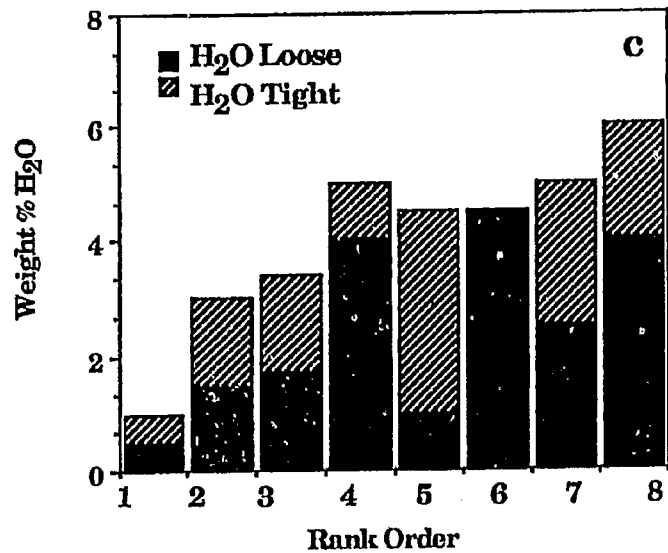
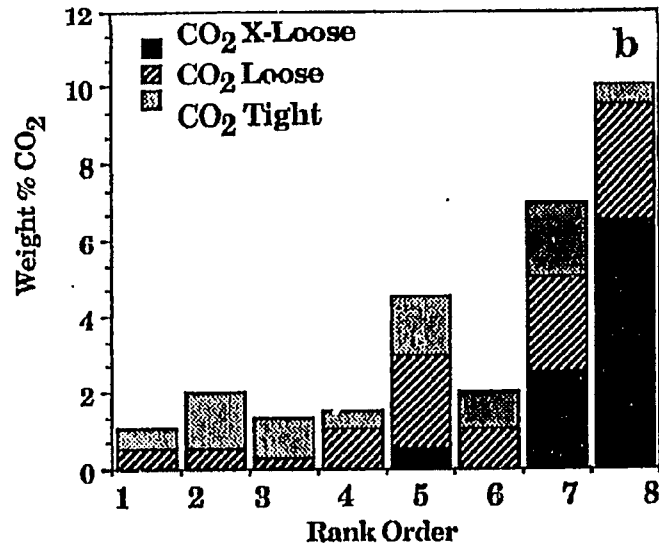
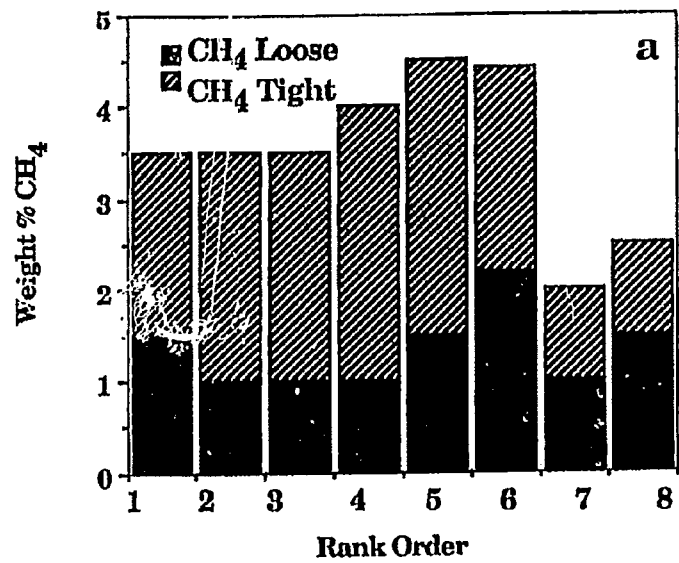


Figure II.A-2. Variation of Functional Group Pools with Rank Order.

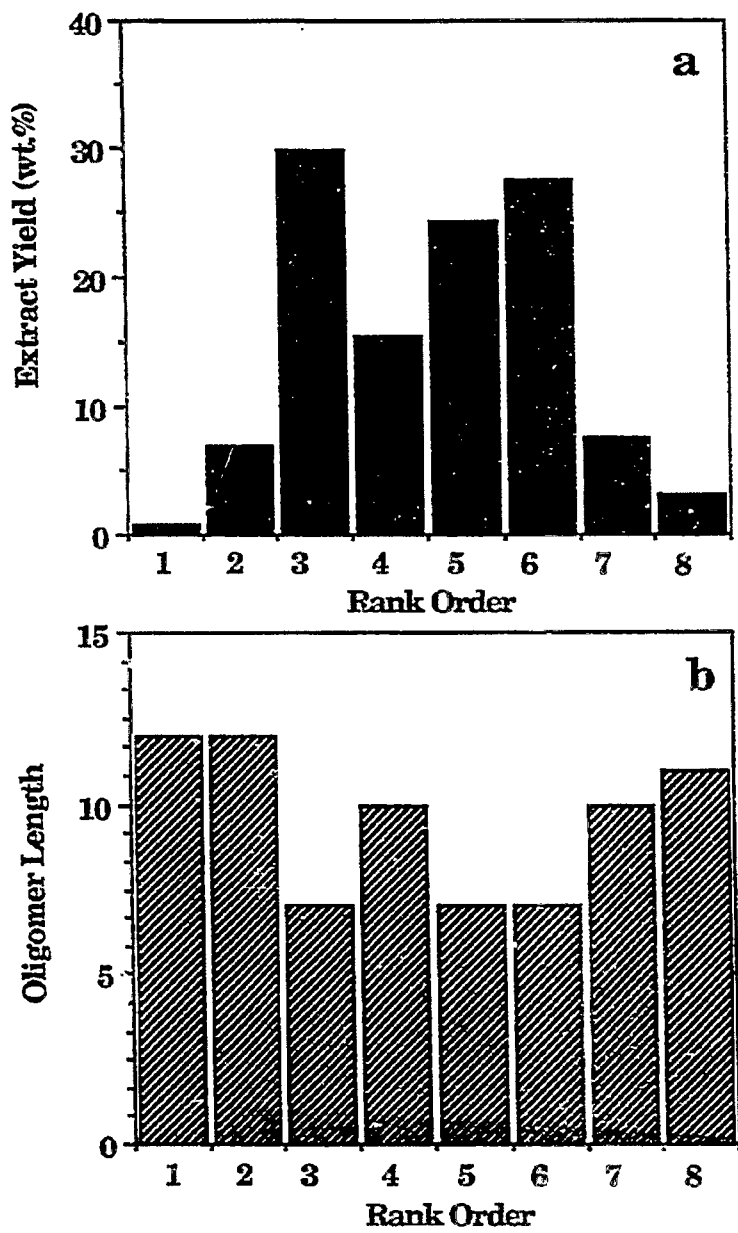


Figure II.A-3. Variation of Extract Yield and Oligomer Length with Rank Order.

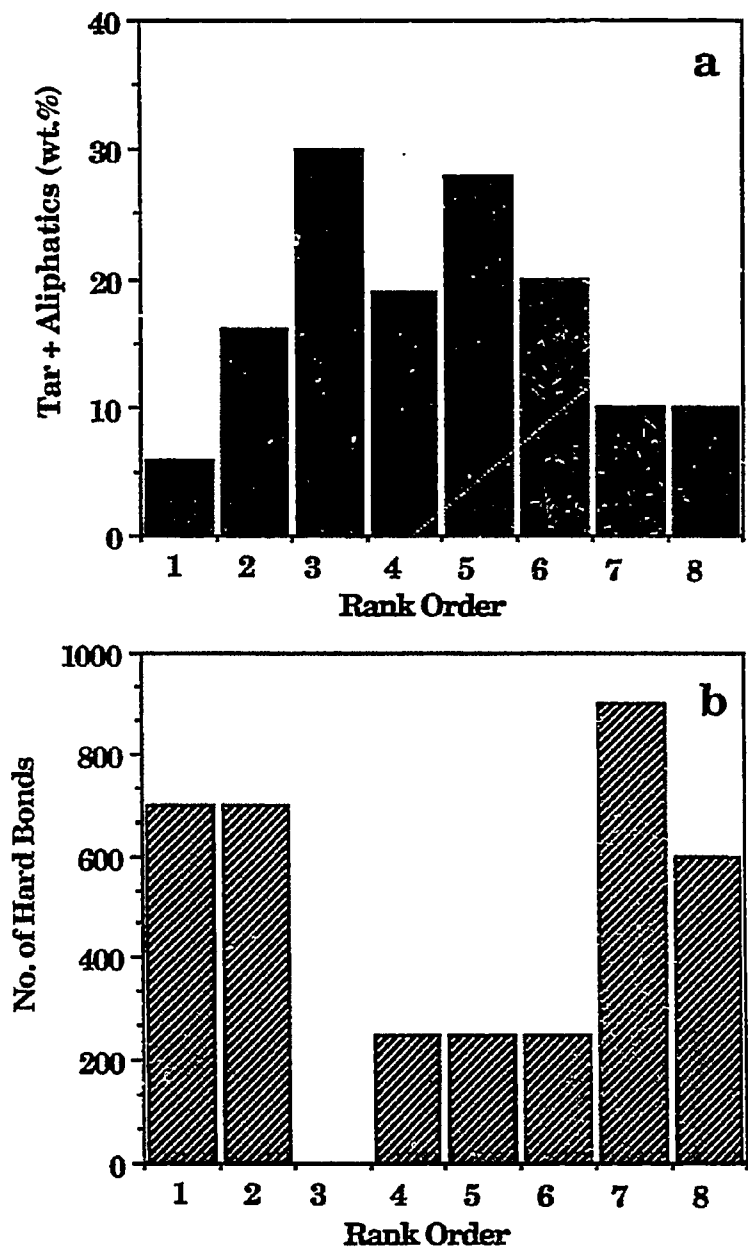


Figure II A-4. Variation of Tar Yield from TG-FTIR Experiment and Number of Hard Bonds with Rank Order.

coals, a value of $\Delta P = 0$ is a good approximation for pressures of one atm or higher. The sensitivity of the model to the choice of ΔP is discussed in a recent paper (Solomon et al., 1988). This is the only parameter in the model which is adjusted for each type of experiment. The original FG model also had a fitting parameter, X_0 , which was used to match the final tar yield to account for differences in particle size, heating rate, bed depth and reactor geometry (Solomon et al., 1988). While it can be said that we have traded one adjustable parameter, X_0 , in the FG model for another, ΔP , in the FG-DVC model, this is not exactly true as the latter model is much richer in its ability to predict a variety of pyrolysis events. The values of ΔP are more restricted than X_0 and have a more fundamental basis that it is related to the coal's viscosity.

The use of the FG-DVC model involves several constraints: 1) Where experimental data are available on the starting coal, such as for the molecular weight between crosslinks (M_c), the extract yield, or the elemental analysis, they are used as inputs. Additional information will be incorporated as it becomes available. 2) The kinetic parameters for the evolution of the FG group pools are assumed to be invariant with coal type. 3) The amounts of the FG pools are constrained to fit data from experiments at very low (0.5°C/s) and very high (5000°C/s) heating rates. This results in a model which is very robust in its ability to fit pyrolysis data over a wide range of conditions. It is also true that when enough coals have been studied, a detailed calibration of the model may not be needed and perhaps the elemental analysis, the particle size and the reactor conditions will be sufficient.

Comparison of Model with Experimental Data

The model is compared with experimental data from the three reactors in Figs. II.A-5 and II.A-6. Except for H_2O , the agreement of the model is generally quite good over a wide range of extents of pyrolysis and for what is a wide range of coal types. A comparison is made between the tar molecular weight distributions measured by FIMS and the predicted values in Fig. II.A-7. The model predicts rank dependent phenomena, such as the steep drop off in the distribution for the low rank coal due to crosslinking events (Solomon et al. 1988).

Conclusions

The conclusions for this work are as follows:

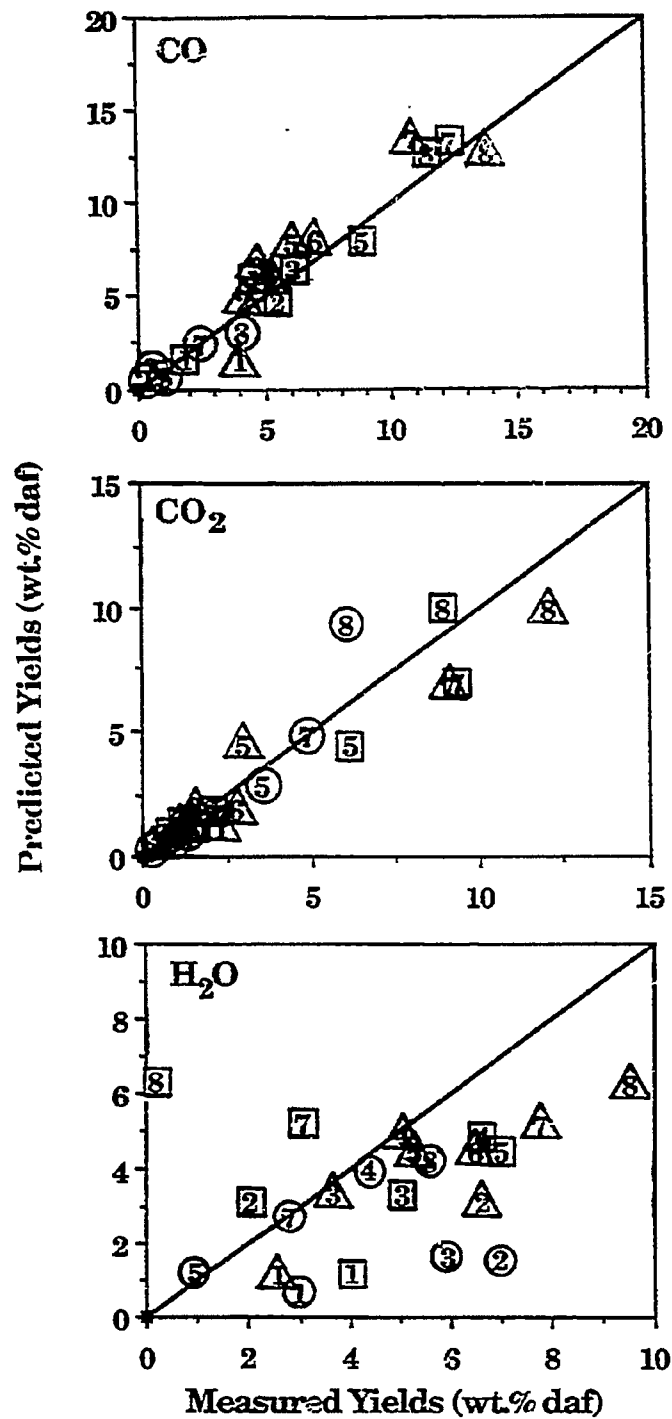


Figure IIA-5. Comparison of Model Predictions with the Data for the Yields of Oxygenated Species. The Numbers Refer to the Coal Type as Given in Table IIA-1. The Symbols Around the Numbers Refer to the Reactor Type. ○ - EFR, 700°C; □ - EFR, 1100°C; △ - TG-FTIR; No Symbol - FIMS.

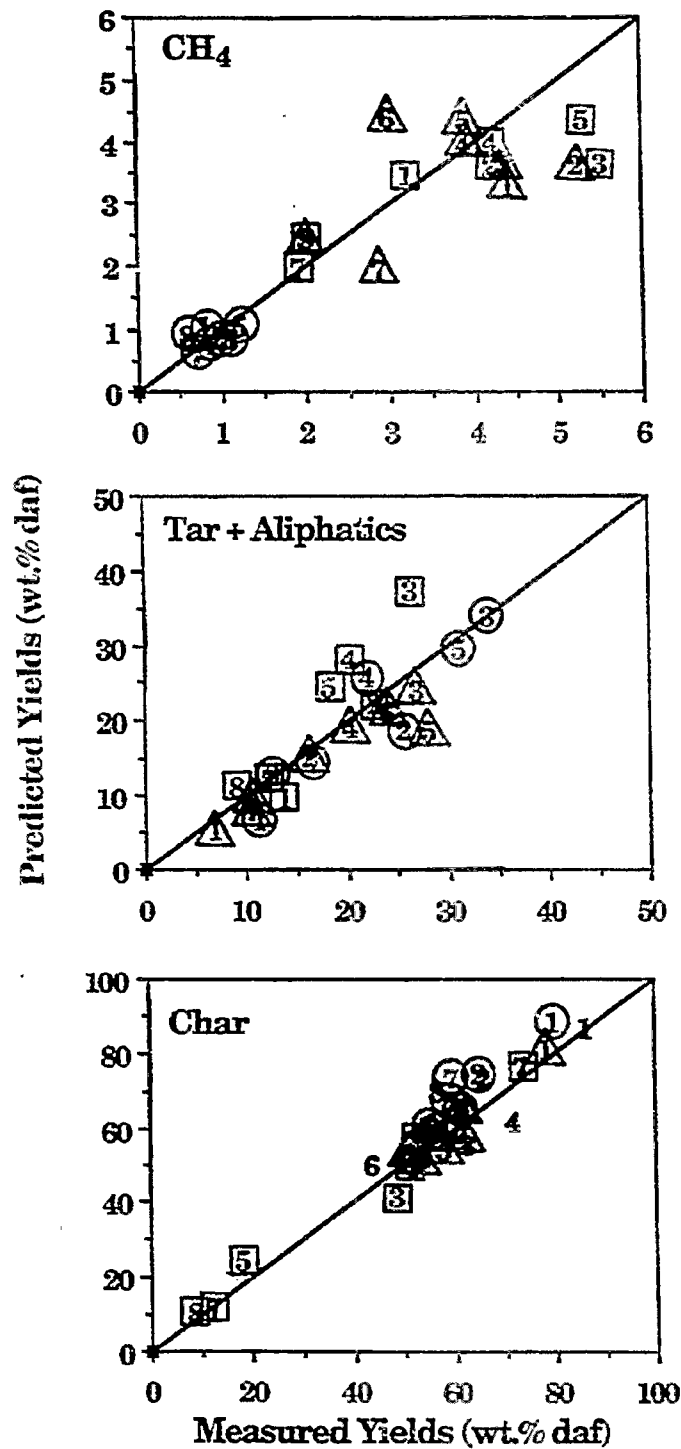


Figure IIA-6. Comparison of Model Predictions with the Data for CH₄, Tar plus Aliphatics, and Char. The Numbers Refer to the Coal Type as Given in Table IIA-1. The Symbols Around the Numbers Refer to the Reactor Type. ○ - EFR, 700°C; □ - EFR, 1100°C; △ - TG-FTIR; No Symbol - FIMS.

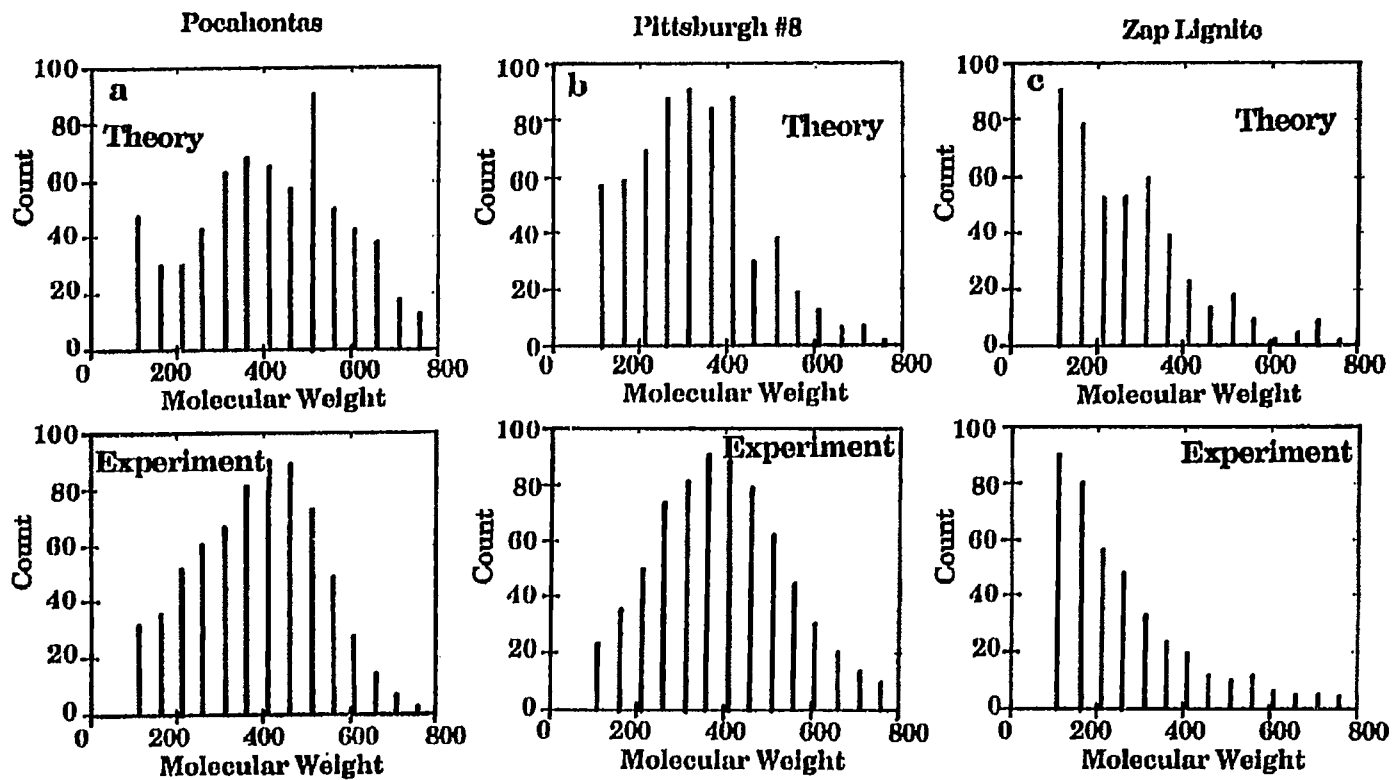


Figure II.A-7. Comparison of Measured and Predicted Tar Molecular Weight Distributions.

- The pyrolysis kinetic data for this series of coals support the assumption of relative rank insensitivity, as does the ability of the model to fit the data using rank independent rates.
- There is a systematic variation in the amounts of individual pyrolysis gases with rank. The oxygenates (CO, CO₂, H₂O) are highest for the low rank coals while the hydrocarbons are highest for the medium rank coals.
- There is a systematic variation in the tar yield and tar molecular weight distribution with rank. The tar yield is highest for medium rank coals. The mean of the tar average molecular weight distribution is highest for the high rank coals. The drop-off in the tar molecular weight distribution is greatest for low rank coals.
- The rank dependent phenomena are well described by the FG-DVC model over a wide range of experimental conditions.

Literature Review of Pyrolysis Data

In order to refine the combined kinetic/mass transport model used for tar in the FG-DVC model, a search was made of literature pyrolysis data obtained for the Pittsburgh Seam bituminous coal. Data from several wire grid experiments with this coal were entered into a spreadsheet program so they could be converted to the same basis and plotted. When a comparison was made of data produced by heating at 1000 K/s to various peak temperatures at one atmosphere pressure, it was found that the results from different investigators did not agree, even when obtained from the same laboratory. These comparisons are shown for the tar yield in Fig. II.A-8.

The difference in kinetic rates implied by these results is more than three orders of magnitude. An even wider variation in results is found when the literature data for weight loss is examined, as shown in Fig. II.A-9. Some of this variation can be attributed to differences in the actual heating profile when compared to the nominal 1000 K/s profile or differences between the various samples of Pittsburgh Seam coal. However, these effects could not account for much more than a factor of 10 in the discrepancies. The major reason for these differences must be the lack of a direct measure of the coal particle temperature in this experiment, which is sensitive to the location and the characteristics of

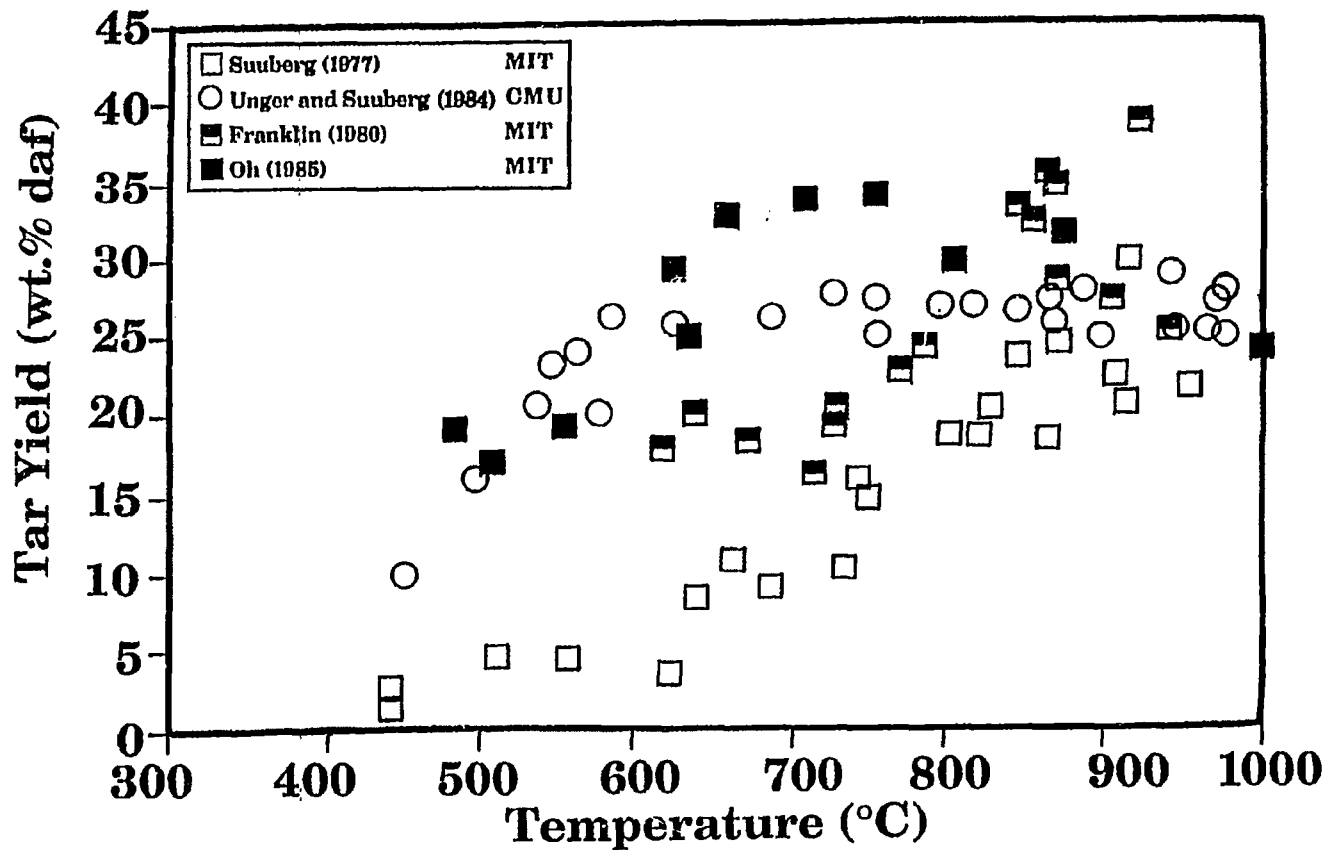


Figure II.A- 8. Comparison of Experimental Tar Yield Data for Non-Isothermal Pyrolysis of Pittsburgh Seam Coal in a Heated Grid. Conditions: 1000 K/s, 1 atm, No Holding Time.

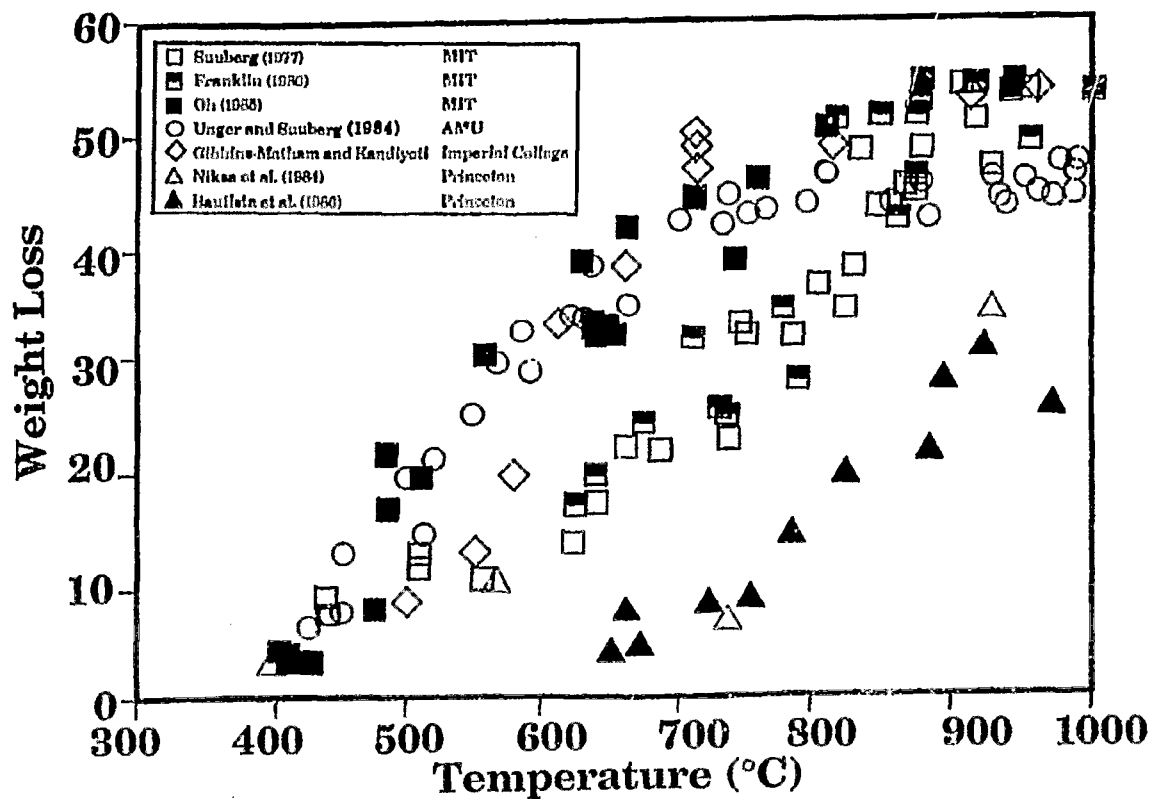


Figure IIA- 9. Comparison of Experimental Weight Loss Data for Non-Isothermal Pyrolysis of Pittsburgh Seam Coal in a Heated Grid. Conditions: 1000 K/s, 1 atm, No Holding Time.

the thermocouple.

The results for the tar kinetic rates implied by these investigators can be summarized in an Arrhenius plot, shown in Fig. II.A-10. The capital letters are estimates for the tar evolution rate obtained by fitting a first order model to the data and evaluating the rate at the temperature where one-half of the tar has evolved. The other data points were obtained at AFR from experiments on a variety of coals at low and high heating rates. The solid lines represent kinetic expressions for tar evolution rates from experiments with model polymers and coal done at AFR. The "AFR TAR RATE" appears to be in the middle of the spread in the literature data and is in good agreement with the data for ethylene-bridged naphthalene polymers.

We began an experimental and theoretical study into possible reasons for the variations in the literature data indicated Figs. II.A-8 to II.A-10, which we are doing in conjunction with Professor Eric Suuberg. The focus of our investigation is currently the location, size and characteristics of the thermocouples used.

Plans

Work will continue on developing a swelling model to go along with the viscosity model which has been integrated into FG-DVC. The TG-FTIR experiment will be recalibrated and the FG-DVC model will be used to predict the differential evolution curves for the standard 30 K/min pyrolysis experiment in this apparatus. The analysis of the literature data on the Pittsburgh Seam coal will continue, with an emphasis on the heated grid experiments.

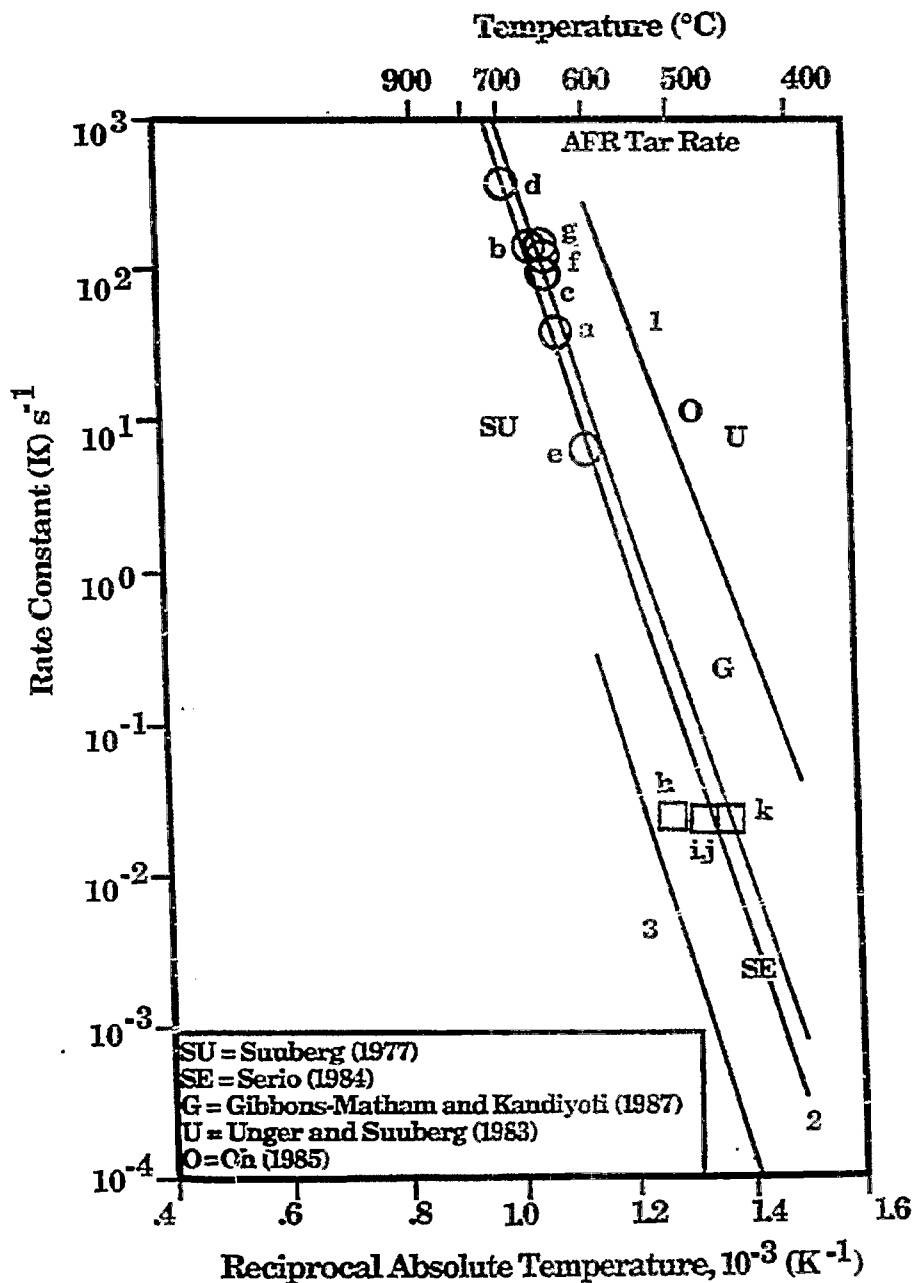


Figure IIA-10. Comparison of Kinetic Rates for Tar Evolution from Coal and Polymers. The Capital Letters are Estimates for the Apparent Kinetic Rate at the Reported Temperature for Reaching One-half the Total Tar Yield for Literature Experiments with Pittsburgh Seam Coal, as Discussed in the Text. The Numbers Next to Each Line Refer to Tar Evolution Rates for: 1) Ethylene-bridged (EB) Anthracene Polymer; 2) EB Naphthalene Polymer; and 3) EB Benzene Polymer. The Data Points are Rates for Tar Evolution from Experiments in the Heated Tube Reactor (HTR) (○) and TG-FTIR (□). The Small Letters Next to Each Data Point Indicate the Coal Type and Experimental Conditions. The Experimental Conditions for the HTR Experiments are Given in Solomon et al. (1986). Coal Types were as Follows: North Dakota (Zap) Lignite (b,c,d,e,k); Montana Rosebud Subbituminous (a,f,i); Illinois No. 6 Bituminous (g,j); Pittsburgh No. 8 Bituminous (h).

**II.B. SUBTASK 2.B. - FUNDAMENTAL HIGH-PRESSURE REACTION
RATE DATA**

Senior Investigators - Geoffrey J. Germane and Angus U. Blackham
Brigham Young University
Provo, Utah 84602
(801) 378-2355 and 6536

Student Research Assistants - Charles Monson and Russell Daines

Objectives

The overall objectives of this subtask are 1) to measure and correlate fundamental reaction rate coefficients for pulverized-coal char particles as a function of char burnout in oxygen at high temperature and pressure and 2) to provide fundamental kinetic rate measurements of sulfur species with sorbents for a range of stoichiometries under laminar, high-pressure conditions.

Specific objectives for the last quarter were to:

1. Continue reactor fabrication and construction.
2. Continue preparation of the test cell to house the reactor and the optical instrumentation.
3. Continue preparation and analysis of test samples of char from Utah bituminous coal under atmospheric and greater than atmospheric pressure.
4. Coordinate char preparation in the high-pressure, controlled-profile reactor with an independently funded study to produce char-tar pairs in the reactor.

Accomplishments

Four components of this subtask have been identified to accomplish the objectives outlined above: 1) char preparation at high temperature and high pressure, 2) determination of the kinetics of char-oxygen reactions at high pressure, 3) design and construction of a laminar-flow, high-pressure,

controlled-profile (HPCP) reactor, and 4) measurements of fundamental sulfur capture rates by sorbents.

Component 1 - Char Preparation at High Temperature and High Pressure

The main objective of this component of the study is to prepare char with three different reactors: (a) a simple hot-tube reactor at atmospheric and elevated pressure and (b) the BYU high-pressure, entrained-flow gasifier and (c) the HPCP reactor being fabricated for this subtask. After the HPCP reactor is completed and tested, char samples will be prepared in this reactor to serve as reference chars to which other char samples from the simple hot-tube reactor and the gasifier can be compared. The purpose of this comparison will be to determine how closely the properties of the chars prepared with the simple reactor and the gasifier parallel the properties of the chars prepared by the HPCP reactor. If the properties are sufficiently close for the same temperatures, pressures, heating rates, and residence times, then confidence in the measured values for the chars prepared with the simple reactor can be achieved. If this can be demonstrated, then chars can be prepared with the simple reactor, and these chars can then be used for the kinetic studies in the HPCP reactor. If this approach is not satisfactory, then both the preparation of the char and the determination of the oxidation kinetics of the char will be carried out in the HPCP reactor.

Chars will be prepared from five different coals from the Argonne premium coal sample bank. Utah bituminous, North Dakota lignite, and Wyoming subbituminous are three of the five coals to be studied; the other two coals will be selected in the near future. A Utah bituminous coal which is similar to but not the same as the Utah coal in the Argonne bank is currently being used to prepare char samples since it is in large supply at the BYU Combustion Laboratory. Small char samples of the Utah coal from the Argonne bank will be characterized and compared to the char samples from the Utah coal.

Literature Review - In this reporting period, consideration was given to the closeness of the particle temperature to the temperature of the walls of the small diameter ceramic tube in the simple hot-tube reactor. It has been assumed in this study that the temperature of the particle passing through the reactor

is the same as the temperature of the wall at that point as measured by a thermocouple. Support for this assumption comes from a study by Solomon et al. (1986) in which it was concluded that the heat transfer between the solids and the gas was so fast that in most cases the thermocouple temperature was predicted to be within 20 degrees C of the coal particle temperatures and that the thermocouple measurement provided a reasonably accurate determination of the particle's temperature history. The inside diameter of the tube in their reactor for very rapid coal pyrolysis was 5 mm compared with an inside diameter of 7 mm used for char preparation in this simple method.

Technical Approach - The simple hot-tube reactor (described in the Fifth Quarterly Report, Solomon et al., 1987), has provided small amounts of char for which CH analyses have been made and scanning electron micrographs (SEM's) have been taken. This hot-tube reactor enables simple changes in the values of heating rate, residence time and temperature. This flexibility will aid in determining the conditions for char preparation in the HPCP reactor. Two runs with the hot-tube reactor at elevated pressure (5 atm) have been conducted. Only small amounts of char were obtained because of plugging of the stainless steel reactor tube which had an inside diameter of 2 mm. This tube is currently being replaced with a stainless steel tube with an 8 mm inside diameter to overcome this problem.

The rationale for the preparation of the char with the simple hot-tube reactor is developed in the following way. The design of the HPCP reactor will enable accurate temperature measurement of the char particle after a period of time at a carefully controlled reaction temperature. The function of temperature control is particularly important in the measurement of the kinetics of char oxidation. In char preparation, however, the temperature control need not be as precise provided the temperature is higher than that to be used in the rate measurements. Therefore, if char samples can be prepared in a less complex reactor with less control of the temperature profile and have essentially the same properties as samples from the HPCP reactor, then it is an advantage to use the simpler reactor for char preparation and the HPCP reactor for the kinetic measurements. Then, more oxidation rate measurements could be made within the time frame for this subtask over a broader range of reaction variables (temperature, residence time, and coal type).

As indicated above, in small-bore reaction tubes, the temperature of the particles is essentially the same as the wall and gas temperatures. Even though the temperature profile of the simple reactor is not controlled, it can be measured (see Figure II.B-1). From the measured temperature profile and the carrier gas flowrate through the reaction tube, residence times and heating rates of the particles undergoing devolatilization can be calculated assuming that the temperature of the particle is the same as the temperature of the wall at that point and that carrier gas and particle velocities are the same. This has been done for some experimental runs as described in the next section.

Analysis and Measurements - Several char samples have been prepared with the simple hot-tube reactor during this reporting period. A char sample from the BYU gasifier was also collected. All of these samples have been analyzed using a CH Analyzer and a few have been analyzed with the Scanning Electron Microscope (SEM). Table II.B-1 lists the preparation conditions of the char samples, such as temperature range (average temperature of the heating zone) and residence time (the amount of time the char spent in the heating zone), as well as the results of the CH analyses. As noted in the Fifth Quarterly Report, it was expected that the hydrogen content of the char sample would decrease as the residence time increased. This trend is generally followed by most of the samples. Some of the samples, however, vary from this pattern. These discrepancies might be due to the fact that they are larger than the other samples. The larger samples required a longer time to collect and more coal to flow down the reactor tube. These two effects caused a build up of char/tar on the inside walls of the reactor tube which effectively reduced the inside diameter. A reduction in the inside diameter of the tube would cause a decrease in the residence time of the particle, resulting in a change of conditions and characteristics for the particles flowing through the narrower tube.

SEM's were taken for the sample from the BYU gasifier and five samples from the simple hot-tube reactor. The micrographs revealed that the char samples from the simple reactor with longer residence times were more porous than those with shorter residence times. This trend is an indication that residence time calculations are reasonably accurate. Also, the char from the gasifier had a much different structure from those obtained from the simple reactor. A non-porous structure was depicted by the micrographs of the char from the

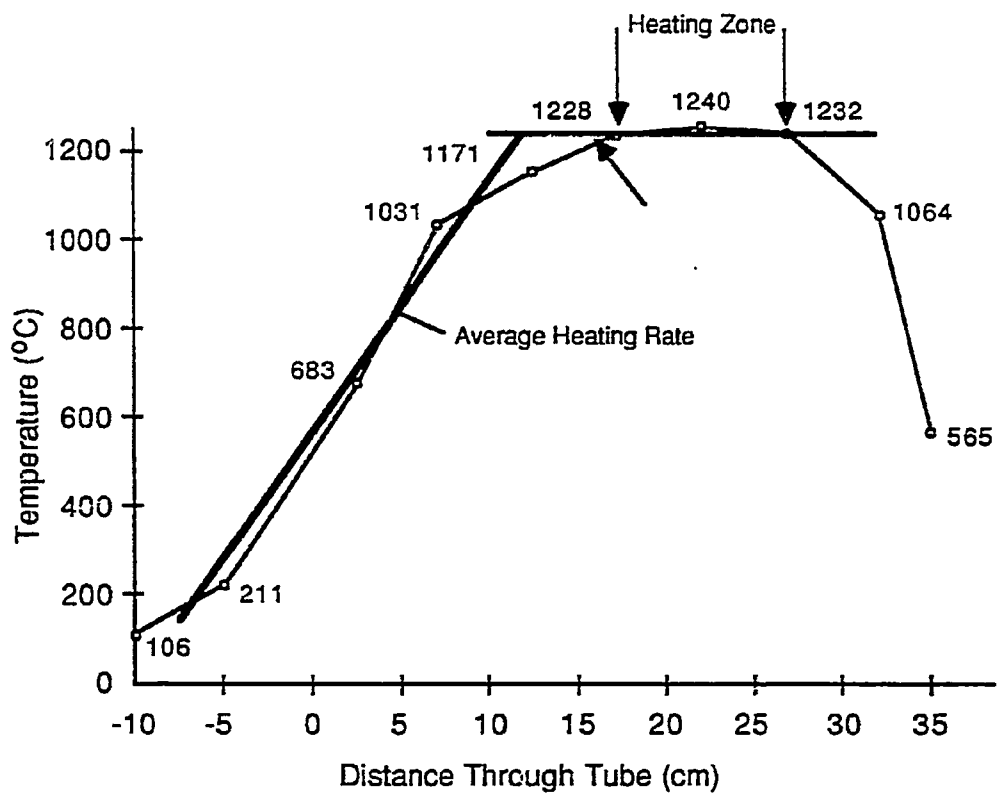


Figure II.B-1. Measured temperature profile of the simple hot-tube reactor.

Table II.B-1
Char Sample Characteristics

Sample	Temperature range (C)	Residence time(ms)	CH Analysis	
			%C	%H
Utah Coal	-----	--	74.7	5.68
Gasifier-1*			76.2	0.96
13	1140-1200	28.4	76.6	2.00
15	1140-1200	28.7	73.6	0.96
12	1140-1200	35.9	79.6	0.36
7	1140-1200	41.1	79.0	0.60
11	1140-1200	53.9	77.4	0.49
6	1192-1211	28.4	79.2	2.55
16	1192-1211	28.7	74.3	1.08
24	1192-1211	61.6	78.1	0.42
23	1192-1211	71.9	81.4	0.16
36	1196-1239	27.8	73.6	1.87
35	1196-1239	29.7	72.6	2.57
32	1196-1239	41.7	76.0	0.27
33	1196-1239	41.7	79.8	0.27

*Obtained from the gasifier. The other char samples were prepared in the simple hot-tube furnace.

gasifier. The micrographs show particles with a wide range of diameters. This is probably due to the fact that the coal wasn't fractionated according to particle size prior to preparing the char. The next SEM's taken will be of the fractionated coal and the chars prepared from this coal. These micrographs should indicate whether the original micrographs showed particles of many sizes or if the particles broke or chipped during the char preparation run.

Heating rate calculations based upon the assumptions previously noted in this report have been determined for two experimental runs. The experimental conditions for these calculations are a maximum temperature of 1240 degrees C, a gas flowrate of 1.00 L/min and a reaction tube inside diameter of 7 mm. The temperature profile (see Figure II.B-1) of the reaction tube was measured with a thermocouple. The profile begins with temperatures at 10 and 5 cm above the furnace down through the furnace until the end of the furnace is reached. An average gas flowrate was calculated at 5 cm intervals within the profile. Each flowrate was adjusted for gas expansion due to the fact that the density of the N₂ gas changed with temperature. Heating rates were determined for each 5 cm increment along the reaction tube to the area of the heating zone. The average heating rate was 10,850 K/sec and the maximum rate of 12,500 K/sec occurred between the 0 and 5 cm interval down the tube. For different gas flowrates with the same temperature profile, the heating rates are multiples of the flowrates. For example, a flowrate of 1.50 L/min produces average and maximum heating rates of 16,250 and 18,700 K/sec, respectively.

Component 2 - Kinetics of Char-Oxygen Reactions at High Pressure

No work conducted during report period.

Component 3 - High-Pressure Reactor Design and Fabrication

The primary objectives of this subtask are to prepare char at high temperature and pressure, to determine the kinetics of char-oxygen reaction at high pressure, and to measure fundamental sulfur capture rates by sorbents at high pressure. The high-pressure, controlled-profile (HPCP) reactor will be used to prepare char, to conduct char reaction rate experiments, to conduct experiments concerning sorbent capture of sulfur species, and to produce and

collect tars. The reactor will operate at pressures up to 27 atmospheres and temperatures up to 1700 K. Provision is made for adjusting the axial temperature profile, in-situ measurement of particle temperature, diameter, and velocity, direct sampling of particles, and variable reaction tube diameters. The general design of the HPCP reactor has been presented in detail in previous quarterly progress reports.

Literature Review - Young et al. (1988) described a new atmospheric pressure char oxidation furnace at the University of North Dakota, the reaction tube consisting of an 8.6-cm-square quartz chimney through which optical measurements were made. A 69-mm lignite char was oxidized in atmospheres containing between 0.05 and 0.16 mole fraction of oxygen. It was reported that the difference between particle and gas temperatures increased from 390 to 725 K with increasing mole fraction of oxygen. The gas temperature was about 1000 K for all tests. It was observed that particle-gas temperature differences increased with decreasing particle size.

Final Design Elements - Figure II.B-2 shows the insulation detail for the HPCP reactor. A high-temperature, mullite fiber layer of insulation will surround the wall heaters. The space between this insulation and the shell will be filled with a castable refractory. Mullite fiber blanket will insulate the preheated gas passageway into the reactor head.

The seal between the reactor head and main section will be created by matching alumina disks. The inner disk will be cemented to the reaction tube while the outer disk will be held in place by the mullite insulation and a cast, high-temperature refractory ring. The flange gasket will extend into the inner portion of the reactor, being cast into the refractory ring at its inner diameter. This will ensure a good seal and prevent the secondary gas from flowing down along the wall heaters and into the reaction tube through the optical holes.

An access port has been added to the lower portion of the preheater shell. This will allow temperature measurements of the preheated secondary gas and monitoring of the Kanthal heaters for control purposes. This access port will

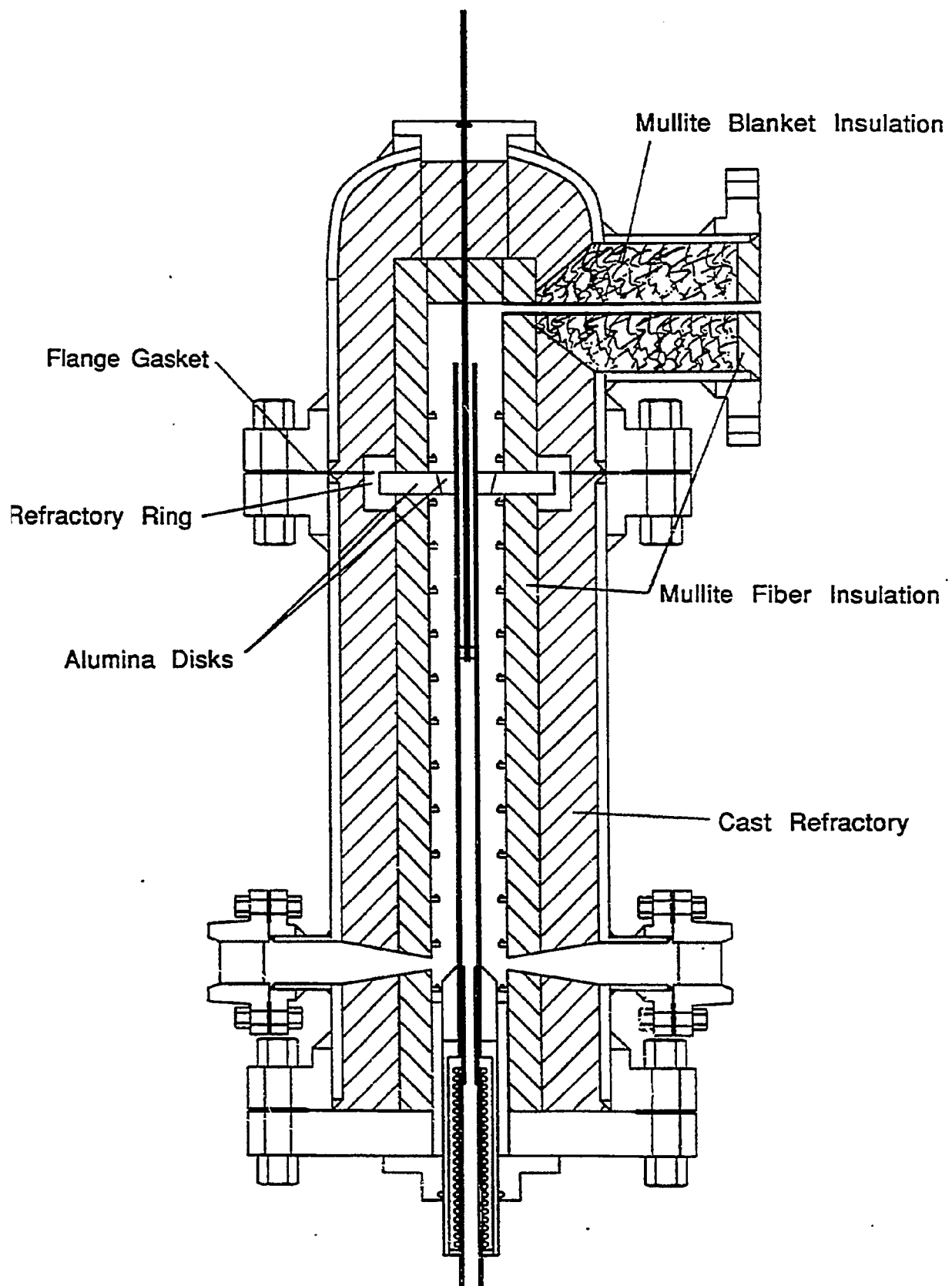


Figure II.B-2. HPCP reactor insulation.

be sealed with a cover identical to the one used at the top of the preheater for the heater access.

In order to provide an isothermal temperature distribution along the reaction tube, the wall heaters will be divided into three heat zones. Each of these zones, as well as the preheater, will be controlled by a phase-angle-fired, silicon-controlled rectifier (SCR) that will receive a control signal from the computer. The computer will monitor thermocouples in each of the heat zones and adjust the silicon-controlled rectifiers to obtain the desired operating temperatures. The number of heaters included in each heat zone will be varied to correspond to the position of the injection tube.

An adjustable stand will bolt to the bottom flange of the HPCP reactor. This stand will allow adjustments to make the reactor vertical and to align it with the optical instrumentation. The stand will attach to a table that will also support the optical components. A wall bracket bolted to the preheater will stabilize the reactor/preheater assembly and provide attachment points for the feeder and injection tube.

A suitable location for the reactor was secured in the BYU engineering building in a test bay designed for high pressure. Required utilities are available at this location and the optical components will stay much cleaner than they would in the basement of the Combustion Laboratory building. This new location is also near another project using a similar optical instrument which will permit sharing of some equipment and optical components with the other project.

Char/Tar Separation - In an independently funded research project, the reactor collection system will be modified to collect and separate the products of coal pyrolysis: tar, char, and gas. The separation system will enhance the quality of the char samples for the char oxidation studies, since it is possible that tar may condense on the char, changing the properties of the char. The new separation system will mostly separate the two components before appreciable tar condensation.

A literature review was carried out to identify other entrained-flow reactors that have been used for tar collection and the methods which were used. Based on the information found, the following modifications and additions will be made to the collection system of the HPCP reactor:

1. A permeable inner liner will be added to the collection probe to allow quench gas to be injected radially along the length of the probe to reduce particle and tar sticking inside the probe.
2. A virtual impactor will follow in line with the collection probe to aerodynamically separate the tar-laden gases from the heavier particles, as shown in Figure II.B-3. The momentum of the char and gas will cause a necessary small amount of carrier gas and tar to be entrained with the char particles, while the tar aerosol will follow the main gas flow to a filter system maintained at room temperature to collect the tar. The flow containing the char will go to a cyclone, sized to remove the char, then to a secondary filter to remove any tar in the flow. The two flows will then rejoin to be exhausted or collected for analysis. Each line will have automatic control valves to keep the flowrates constant to ensure good sampling. A vacuum pump will be used during atmospheric pressure runs, which will also remain in place for the char oxidation tests for char collection.

Instrumentation/Optics - Optical breadboards and a table to support them are being fabricated. No commercially-available optical tables can support the weight of the reactor while providing enough flat table space for the optics. Because the new test cell is located near another project, sharing the data acquisition system and some of the optical components won't be difficult. It is planned to share two photomultiplier tubes with their amplifiers and filters, a laser detector, and a digital oscilloscope. The trigger laser, lenses, apertures, beam splitter, and calibration components will be purchased since their placement relative to each other and the reactor is critical. Because these parts must be aligned and solidly mounted, it would be difficult to share them between two projects. However, sharing some equipment will significantly reduce the cost of the instrument.

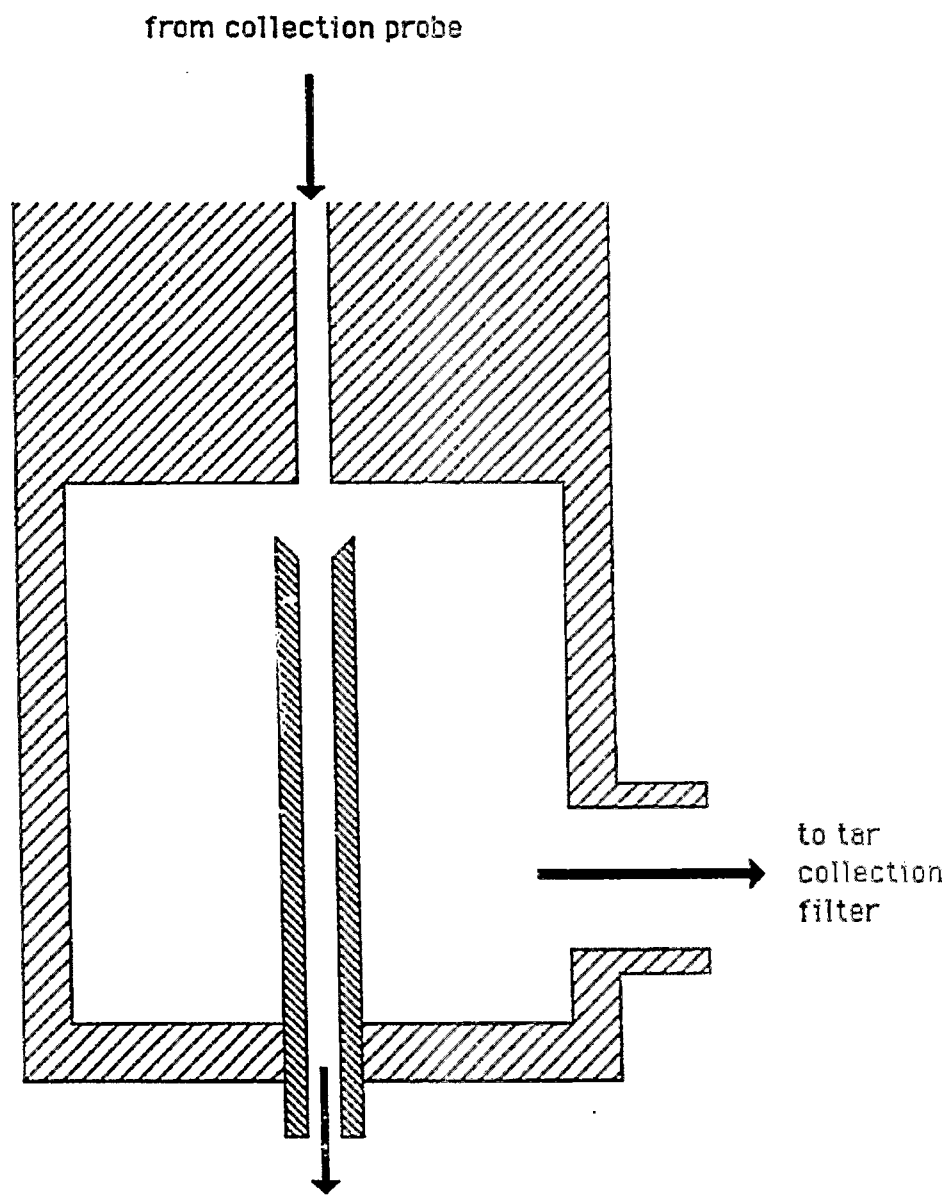


Figure II.B-3. Schematic of virtual impactor for char-ter separation.

Type S thermocouples will measure the gas and heater temperatures along the reaction tube and at the preheater exit. These temperatures will be collected by the computer and its acquisition system.

Fabrication/Construction - After extended machine shop delays, fabrication of the reactor and preheater shells was completed at the end of this reporting period. It was necessary to stress-relieve the reactor sections because of the large amount of welding required during construction. Molds for casting the refractory into the reactor sections have also been completed, and nearly all of the insulating materials have been received.

Construction of the reactor stand is also complete. This stand will support and allow adjustment of the HPCP reactor and will bolt to the optical table, which is nearly completed as well. This table will allow adjustment of the optical breadboards and provide vibration isolation from the floor.

Component 4 - Fundamental Sulfur Capture Experiments

No work conducted during the report period.

Other Activities

The research team organized a char preparation and analysis coordination meeting with other research groups at Brigham Young University and The University of Utah who are doing related work under separate funding. Technical presentations were made at the meeting to exchange information concerning char preparation and measurement of char properties, and to initiate an arrangement to share analytical equipment and expertise.

Plans

Additional char for comparison and analysis will be produced in the elevated-pressure, hot-tube reactor. These samples will be prepared in the 8 mm stainless steel tube which is currently being fitted so that it can attach to the present hot-tube reactor. Similar analyses will be performed on these

samples as were performed on the previous char samples, and comparisons will be made from the results. Chars will be made in both the atmospheric and the elevated pressure reactor according to coal particle size. The scanning electron micrographs of the coal, the chars from each simple reactor and the char from the gasifier will be analyzed for similarities and differences.

Figure II.B-4 shows the construction schedule for the HPCP reactor. The basic reactor with support equipment, including the optical table, is planned to be completed during the next quarter. Instrumenting the reactor will begin during the next quarter and will be completed during the following quarter. Testing and characterization will be started in October, 1988, and extend into December, 1988, when char testing will begin. Char will be prepared in the HPCP reactor during and following reactor testing and characterization.

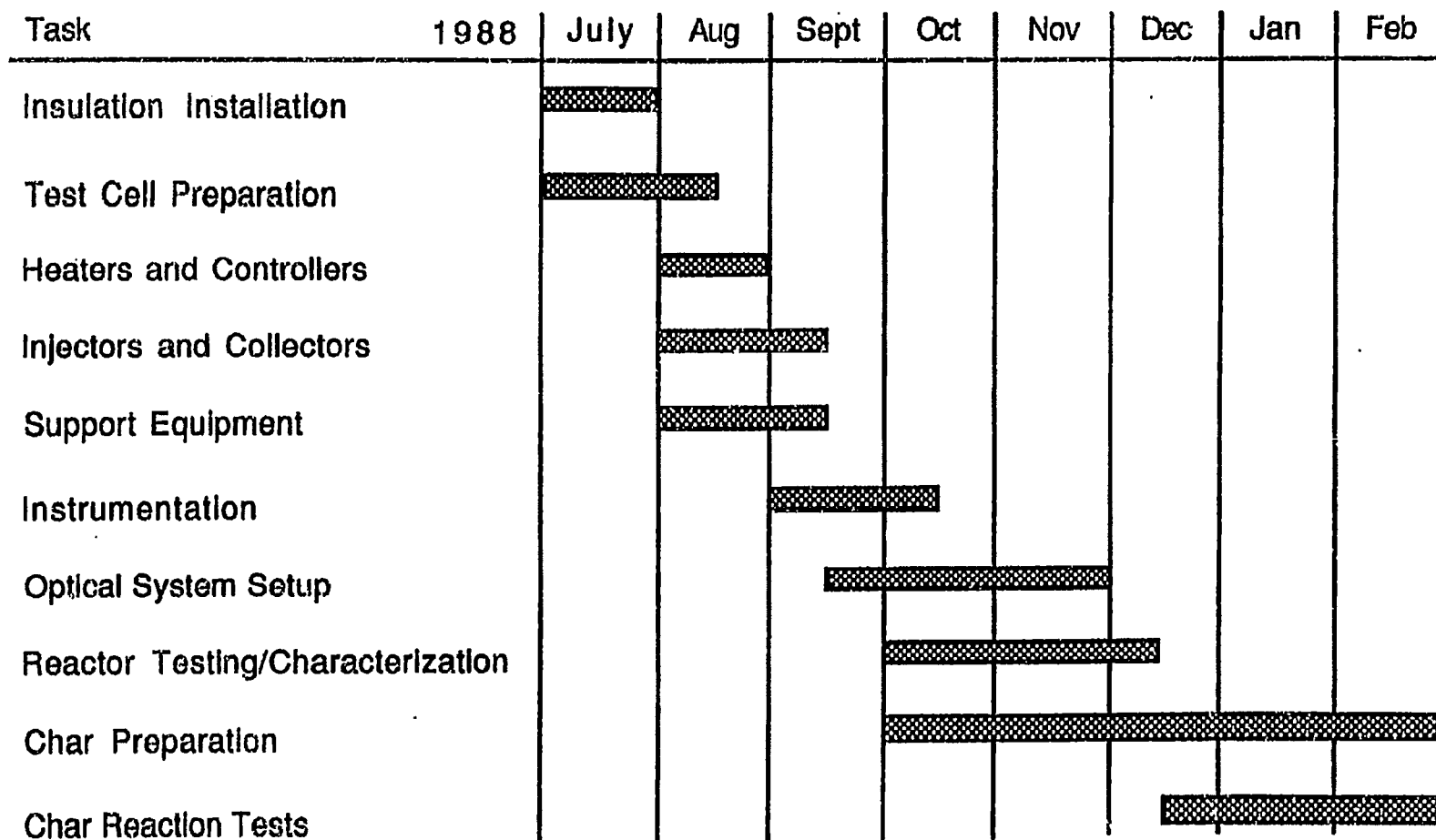


Figure II.B-4. HPCP reactor construction schedule

**II.C. SUBTASK 2.c. - SECONDARY REACTION OF PYROLYSIS PRODUCTS AND CHAR BURNOUT
SUBMODEL DEVELOPMENT AND EVALUATION**

Senior Investigator - Michael A. Serio
Advanced Fuel Research, Inc.
87 Church Street, East Hartford, CT 06108
(203) 528-906

Objective

The objective of this subtask is to develop and evaluate by comparison with laboratory experiments, an integrated and compatible submodel to describe the secondary reactions of volatile pyrolysis products and char burnout during coal conversion processes. Experiments on tar cracking, soot formation, tar/gas reaction, char burnout, sulfur capture, and ignition will be performed during Phase I to allow validation of submodels in Phase II.

Accomplishments

Data collection was temporarily suspended in the TWR as the spectrometer was needed for a different project. Some of the work done previously in this program was summarized in a paper accepted for presentation at the 22nd Symposium (Int) on Combustion in Seattle, Washington (Aug., 1988) which is included as Appendix A.

Plans

Continue data collection in TWR for ignition and burnout experiments with chars, coals and demineralized coals.

II.D. SUBTASK 2.d - ASH PHYSICS AND CHEMISTRY SUBMODEL

Senior Investigator - James Markham
Advanced Fuel Research, Inc.
87 Church Street, East Hartford, CT 06108
(203) 528-906

Objective

The objective of this task is to develop and validate, by comparison with laboratory experiments, an integrated and compatible submodel to describe the ash physics and chemistry during coal conversion processes. AFR will provide the submodel to BYU together with assistance for its implementation into the BYU PCGC-2 comprehensive code.

To accomplish the overall objective, the following specific objectives are: 1) to develop an understanding of the mineral matter phase transformation during ashing and slagging in coal conversion; 2) To investigate the catalytic effect of mineral matter on coal conversion processes. Emphasis during Phase I will be on the acquisition of data which will be utilized for model development in Phase II. Data acquisition will be focused on: 1) design and implementation of an ash sample collection system; 2) developing methods for mineral characterization in ash particles; 3) developing methods for studying the catalytic effect of minerals on coal gasification.

Mineral matter in coal is a source for slagging and deposits on reactor or down stream component walls, causing corrosion of equipment. Minerals can also catalyze reactions or can poison processing catalysts. The objective of this research is for the development of a model for the prediction of ash behavior and the correlation of the behavior with the original chemical composition, particle size, physical properties of the minerals and the process conditions. A model will also be developed to predict the catalytic effect of minerals on coal conversion.

Accomplishments

In order to further understand the role played by ion-exchanged cations on char reactivity, samples of demineralized Zap coal were subjected to ion-exchange experiments with Ca, Na, and K. Ca exhibited a saturation effect, while Na and K

exhibited a maximum in reactivity with increased loading.

Char Reactivity

Investigations to further understand the effects of the ion-exchangeable cations on char reactivity were continued in this quarter. A 200 x 325 mesh sieved fraction of Zap Indianhead, demineralized according to the standard Bishop and Ward (1958) technique, was subjected to ion-exchange with Ca, Na, and K using the modified Hengel and Walker (1984) procedure described in the Sixth Quarterly Report. The amount of cation exchanged onto the demineralized Zap was controlled by varying the molarity of the acetate salt solutions. In the case of Ca, 0.1 M and 0.3 M solutions were employed, while, in the cases of Na and K, 0.1 M, 0.3 M as well as 1.5 M solutions were used.

The amount of cation exchanged was determined by x-ray analysis. The mineral components for the raw and cation-loaded samples are listed in Table II.D-1.

Char reactivity measurements (T_{CR}) were done in air on chars prepared by heating in N_2 at 30°C/min to 900°C and the results are given in Table II.D-2.

In Fig. II.D-1, T_{CR} (°C) is plotted against wt% Ca for the raw, demineralized and the 0.1 M, 0.3 M, 0.5 M, 1.0 M, and 1.5 M loaded (demineralized) Zap samples. The only significant change in reactivity occurs when the Ca level increases from 0.01 wt% in the demineralized Zap to 1.26 wt% in the raw Zap. Further increases in Ca do not cause any marked increase in reactivity.

The 0.1 M Na and K loadings were so effective in promoting the demineralized Zap char reactivity that the loaded samples yielded values of T_{CR} that were 45°C and 30°C respectively less than the T_{CR} of the raw Zap char itself (see Figs. II.D-2 and II.D-3). With higher loadings however, both Na and K lost their ability to increase char reactivity (lower the T_{CR}) and actually demonstrated hindering effects. The 1.5 M Na and K loadings gave values of T_{CR} which were higher by 129°C and 85°C, respectively, than the demineralized Zap sample. We had some surface area measurements done of the raw and cation-loaded samples in these cases. However, significant differences were not observed between the raw and cation-loaded coals in either case. Consequently, the hindering effect must manifest itself during the char formation process. We plan to check this by doing pyrolysis experiments with cation-loaded samples in a reactor which can handle samples which are large enough to allow surface area measurements on the resultant

Table II.D-1. Mineral Components in Raw, Demineralized and Cation Loaded Demineralized Zap Indianhead Samples.

	Raw Zap	Demin. Zap	0.1M Ca Loaded Demin. Zap	0.3M Ca Loaded Demin. Zap	0.1M Na Loaded Demin. Zap	0.3M Na Loaded Demin. Zap	1.5M Na Loaded Demin. Zap	0.1M K Loaded Demin. Zap	0.3M K Loaded Demin. Zap	1.5M K Loaded Demin. Zap
Na	0.13	0.00	0.00	0.00	0.55	0.72	2.15	0.00	0.00	0.02
Mg	0.46	0.05	0.05	0.05	0.04	0.08	0.06	0.04	0.05	0.05
Al	0.46	0.05	0.04	0.04	0.03	0.04	0.04	0.04	0.03	0.03
Si	0.84	0.17	0.16	0.12	0.16	0.12	0.10	0.15	0.13	0.05
K	0.04	0.02	0.00	0.00	0.00	0.00	0.00	1.47	1.64	3.85
Ca	1.26	0.01	1.63	2.49	0.01	0.03	0.03	0.02	0.02	0.31
Ti	0.04	0.00	0.00	0.00	0.00	0.00	0.00	0.01	0.07	0.01
S(o)	0.47	0.52	0.38	0.43	0.49	0.38	0.40	0.47	0.38	0.40
S(m)	0.31	0.15	0.10	0.15	0.10	0.19	0.09	0.14	0.12	0.10
Fe*	0.45	0.04	0.04	0.03	0.07	0.00	0.03	0.05	0.04	0.03
Ash	8.62	0.72	3.99	5.45	2.23	2.55	6.44	2.52	2.66	6.16

* Non-pyritic

Table IID-2. Reactivity Measurements for Raw, Demineralized and Cation Loaded Demineralized Zap Indianhead Samples.

	0-900°C N ₂ Char T _{cr} (°C) in Air
Raw Zap	418, 420
Demineralized Zap	542, 540
0.1M Ca Loaded Demin. Zap	420
0.3M Ca Loaded Demin. Zap	413
0.1M Na Loaded Demin. Zap	380, 373
0.3M Na Loaded Demin. Zap	492
1.5M Na Loaded Demin. Zap	669
0.1M K Loaded Demin. Zap	392
0.3M K Loaded Demin. Zap	534
1.5M K Loaded Demin. Zap	625

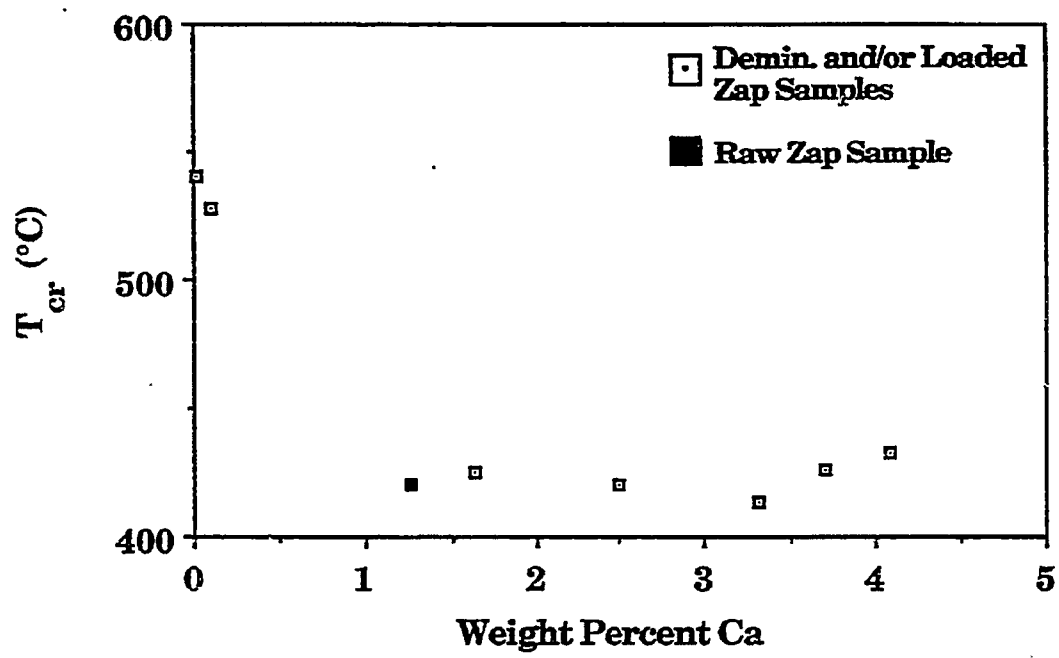


Figure IID-1. Variation of Reactivity with Weight Percent Calcium in the Parent Coal.

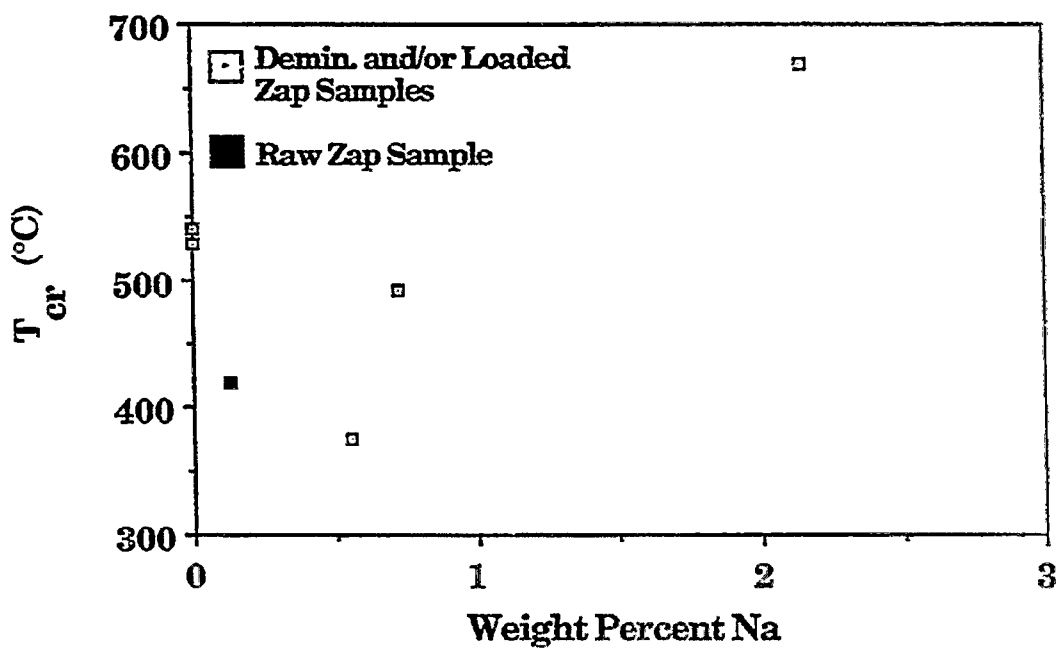


Figure ILD-2. Variation of Reactivity with Weight Percent Sodium in the Parent Coal.

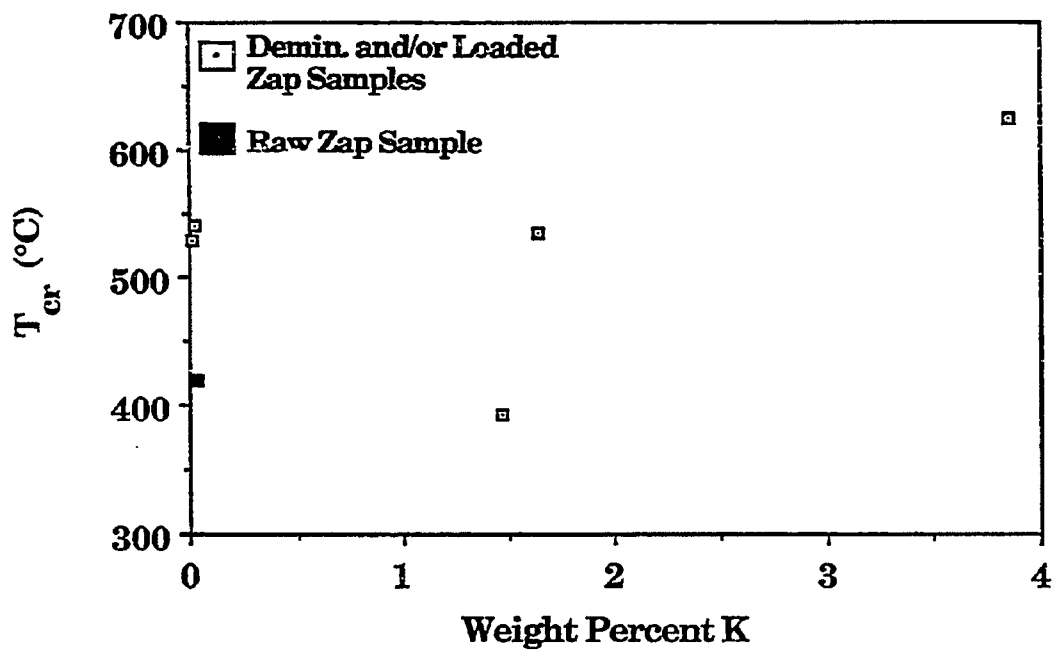


Figure ILD-3. Variation of Reactivity with Weight Percent Potassium in the Parent Coal.

char.

Plans

Continue analysis of mineral effects on char reactivity.

II.E. SUBTASK 2.e. - LARGE PARTICLE SUBMODELS

Senior Investigator - Michael A. Serio
Advanced Fuel Research, Inc.
87 Church Street
East Hartford, CT 06108
(203) 528-9806

Objective

The objectives of this task are to develop or adapt advanced physics and chemistry submodels for the reactions of large coal particles (> 0.5 mm) and to validate the submodels by comparison with laboratory scale experiments. The result will be coal chemistry and physics submodels which can be integrated into the fixed-bed (or moving-bed) gasifier code to be developed by BYU in Subtask 3.b. Consequently, this task will be closely coordinated with Subtask 3.b.

Accomplishments

The construction of the fixed-bed reactor was nearly completed. Discussions were held with Dr. Radulovic (from BYU) on the relationship between the fixed-bed reactor model and the large particle pyrolysis model.

Interface of Single Particle and Reactor Models

Historically, some fixed-bed gasifier models have assumed the devolatilization process to be instantaneous. Others have included finite rates for devolatilization and secondary reactions. The literature review by BYU identified three properties the devolatilization model should be able to predict: 1) the individual chemical species that will be evolved; 2) the amount of each that will be evolved; 3) the rate at which each will be evolved as a function of the pertinent variables (particle size, temperature, heating rate, pressure, gas velocity).

Currently, the FG-DVC model does a good job of predicting the kinetics and yields for the major products for a specified time-temperature history and pressure. What will be required for the fixed-bed model is to describe the devolatilization of large particles which may have significant internal gradients because of their large size and/or may react at significantly different times

because of the broad size distribution of particles. These two effects could be accounted for by using a set of representative particles of different sizes as is done in PCGC-2. Instead of different trajectories the model would need to account for particles at different radial positions. This concept is shown schematically in Fig. II.E-1. One could also use continuous distribution functions instead of discrete distributions for particle size and location.

Other areas to be addressed include multiple particle effects, such as agglomeration, the secondary reactions of tar in the vapor space and on external surfaces, and the char reactivity. It may be possible to ignore agglomeration since most fixed-bed reactors have mechanical devices to prevent this. However, agglomeration may be important in mild gasification processes. Because of the lack of appropriate data, it is difficult to say how the secondary cracking of tar on surfaces should be treated. It is hoped that sufficient data to describe this phenomena will be generated under this subtask (2.e). The description of char reactivity will be an extension of the work done on smaller particles under subtask 2.a.

Discussions were held at AFR during the past quarter between Predrag Radulovic of BYU and Michael Serio, Peter Solomon, and Zhen-Zhong Yu of AFR regarding the interface between the Single Particle Devolatilization Model and the Fixed-Bed Reactor model. The consensus was that the interface would be very similar to that between the FG-DVC model and the 87 version of the PCGC-2. The major differences would be the requirement for a non-isothermal particle temperature model. The major area of uncertainty is how to efficiently integrate the non-isothermal particle model with the FG-DVC model to provide an "averaged" pyrolysis product distribution and char reactivity for large particles. As the two models are developed in parallel, a sensitivity analysis will help define what information should be exchanged and the degree of sophistication required. It was generally agreed that the amount of calculation time for the pyrolysis model should be less than 25% of the total.

This meeting also addressed the differences which may be required in the case of modeling a fixed-bed mild gasification unit, which are likely to be transient, batch systems with stronger particle interactions. The model will need to be flexible enough to cover these situations.

Top View of Fixed-Bed Reactor

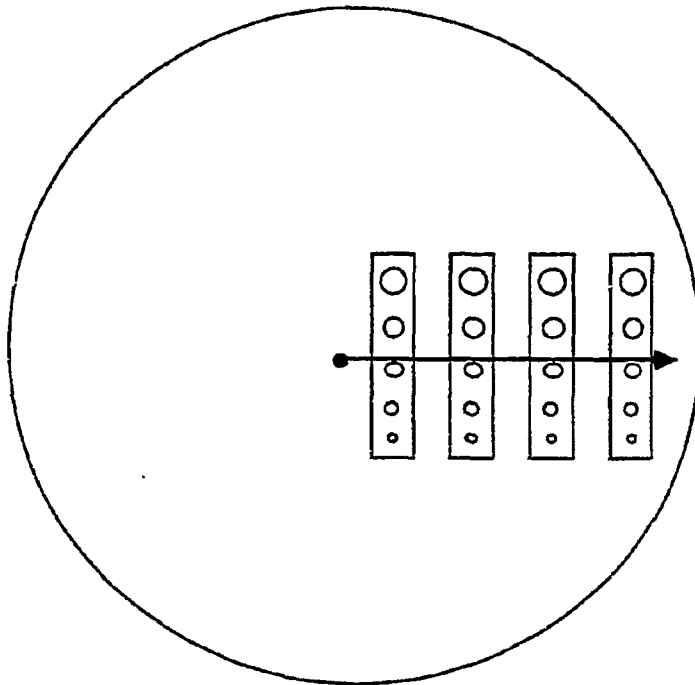


Figure ILE-1. Proposed Method for Incorporation of Single Particle Model into Fixed-Bed Reactor Model Using Five Representative Particle Sizes at Four Representative Particle Locations.

Plans

Complete construction of fixed-bed reactor and begin testing. Begin model development for large particle submodel. Continue work with BYU on interface of this model with the BYU fixed-bed model. Consider the specific needs for modeling mild gasification processes.

II.F. SUBTASK 2.f. - LARGE CHAR PARTICLE OXIDATION AT HIGH PRESSURES

Senior Investigator - Angus U. Blackham
Combustion Laboratory
Brigham Young University
Provo, Utah 84602
(801) 378-2355

Objective

Provide data for the reaction rates of large char particles of interest to fixed-bed coal gasification systems operating at pressure.

Accomplishments

No work planned.

Plans

No work planned.

II.G. SUBTASK 2.G. - SO_x/NO_x SUBMODEL DEVELOPMENT

Senior Investigators - L. Douglas Smoot and B. Scott Brewster
Brigham Young University
Provo, Utah 84602
(801) 378-4326 and 6240

Graduate Research Assistant - Richard Boardman

Objectives

The objectives of this subtask are 1) to extend an existing pollutant submodel in PCGC-2 for predicting NO_x formation and destruction to include thermal NO, 2) to extend the submodel to include SO_x reactions and SO_x-sorber reactions (effects of SO₃ nonequilibrium in the gas phase will be considered), and 3) to consider the effects of fuel-rich conditions and high-pressure on sulfur and nitrogen chemistry in pulverized-fuel systems.

Accomplishments

During the past quarter, computer simulations were made of an entrained-flow coal/oxygen gasifier and a turbulent-jet propane/air diffusion flame in order to evaluate the combined thermal NO and fuel NO submodel development. The results of the coal reactor case were favorable, showing an improvement of the predicted NO concentrations over the fuel NO mechanism exclusively. NO_x prediction for the propane flame case was improved where the predicted temperature and oxygen concentrations were reasonable.

A thorough review was made of alternative fuel-NO global mechanisms. A kinetic path including ammonia species as an intermediate is being sought to potentially improve prediction of fuel NO formation from low-rank coals. A survey of on-going SO_x research was also continued to identify the important elements of a SO_x submodel capable of predicting the conversion of fuel-bound sulfur to gas species.

Component 1 - NO_x at High-Pressure/Fuel-Rich Conditions

The goal of this subtask component is to extend the current pollutant submodel in the comprehensive code to be applicable to high-pressure, fuel-rich

conditions such as are common in gasification processes. An important part of this extension is the inclusion of thermal NO formation which may be significant at the higher temperatures typical of gasification in oxygen.

Prediction Results/Model Evaluation - The BYU entrained-flow gasifier was simulated to evaluate the combined thermal NO and fuel NO submodel. The case examined was for fuel-rich gasification (stoichiometric ratio ~ 0.4) of Utah Bituminous coal at a coal feed rate of 34 kg/hr (Brown et al., 1986). Figure II.G-1a shows the calculated centerline temperature profile for this case. Figure II.G-1b compares the predicted and measured centerline NO_x profiles. Heat loss was assumed to be 40 percent throughout the reactor. Inclusion of the thermal NO mechanism in the model clearly improves the agreement of the predicted NO_x concentrations with the measured data. The predicted peak NO value was increased by approximately 20% and closely matches the measured quantity in the early reactor region. The predicted flame structure shows a high peak temperature where early coal volatiles are rapidly released. This is followed by a fuel-rich, oxygen-depleted zone where the temperature is reduced and also where the predicted rate of NO formation is negligible. Then, as oxygen mixes in, the rate of NO formation again increases. The experimental NO data do not resolve this fuel-rich zone. The comparison of experimental and predicted NO data do, however, compare reasonably well in the early and mid-reactor regions. The theoretical contribution of thermal NO is largest in zones where temperature is high and oxygen concentrations are appreciable.

In order to carefully evaluate the mechanism for thermal NO in the NO_x model, it is desirable to make comparisons between predicted and experimental NO concentrations in gaseous, fuel-nitrogen-free, combustion systems. A literature survey of experimental thermal NO investigations was described in the 5th Quarterly Report (Solomon et al., (1987)). Simulation of these laboratory devices requires specification of the reactor geometry and inlet feed conditions. PCGC-2 is currently only applicable to fully turbulent, axi-symmetric flow reactors. Detailed profiles of the temperature, major species, and NO concentration are necessary to confidently make an evaluation of the model performance. None of the available data reported previously were judged to be completely suitable according to these criteria. The experimental investigation of Takagi and Ogasawara (1981) of a turbulent-jet propane fuel and

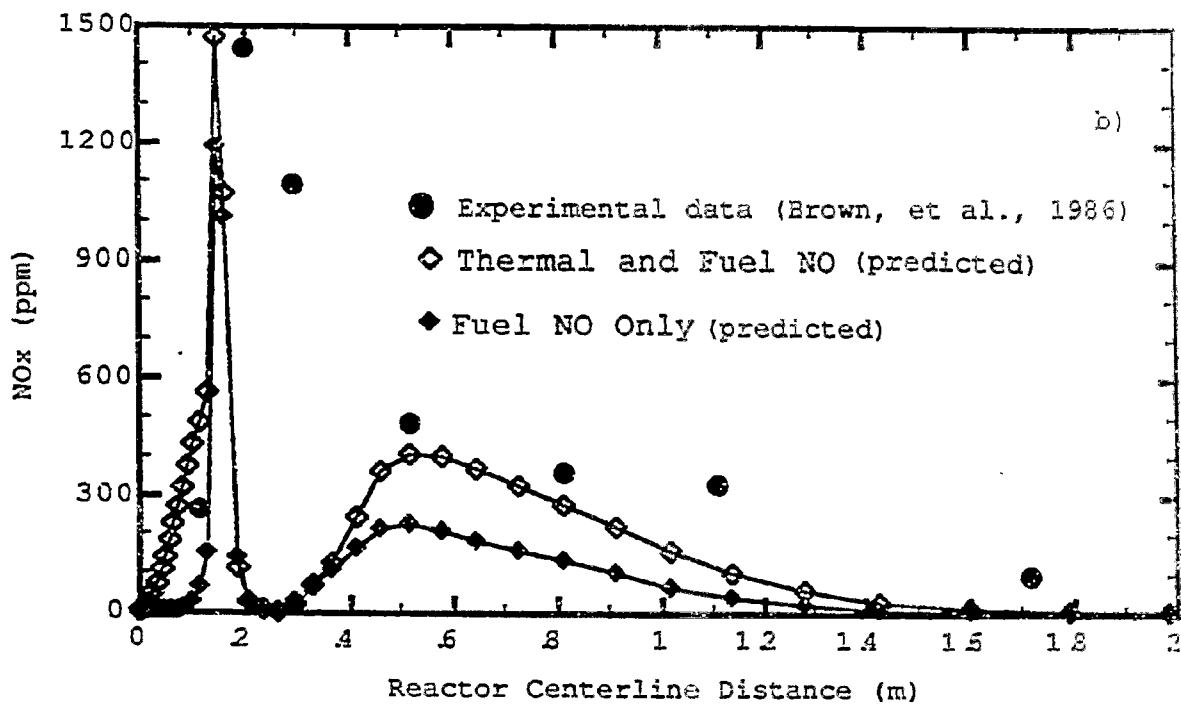
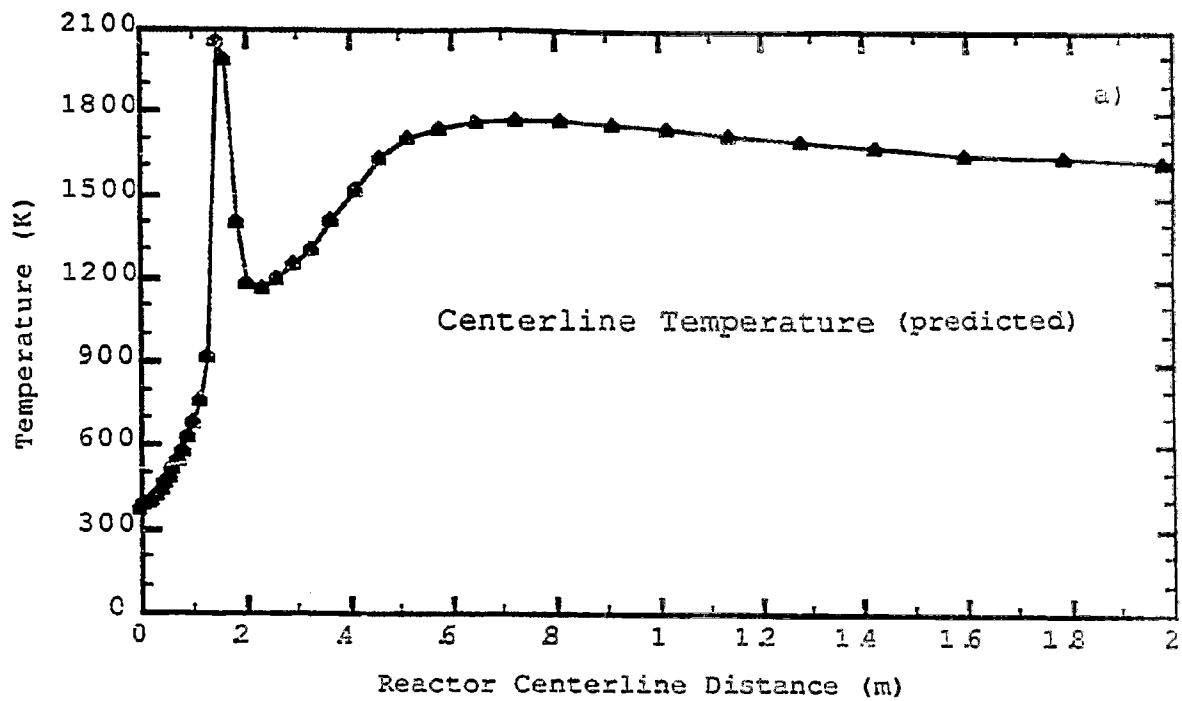


Figure II.G-1. Predicted axial temperature, pollutant profiles, and experimental data for gasification of Utah bituminous coal.

laminar coflowing air stream was selected for model prediction since major species, pollutant, and temperature profiles, although limited, were reported as well as adequate information to simulate the reactor. A reactor schematic is shown in Figure II.G-2. The major limitation of this case is the ability of PCGC-2 to accurately model the mixing of the laminar air and the turbulent fuel jet. This experimental investigation, however, is not unlike many other studies in which a similar laboratory burner was used.

The results shown in Figure II.G-3 compare measured temperature, CO_2 , CO , H_2 , H_2O , and O_2 profiles at an axial location of 200 mm to predicted profiles at 200 mm and 150 mm. The measured profile at 200 mm agrees more closely to the predicted profiles at the axial location of 150 mm. At an axial distance of 200 mm, the theory overpredicts the extent of fuel oxidation and product formation, presumably due to incorrect prediction of the mixing. The high predicted temperature at 200 mm is reflected in the thermal NO_x profile which exceeds the data by 200 ppm at the peak. Predictions at the axial location of 150 mm more closely match the measured temperature and species profiles at 200 mm. The predicted NO_x profile also closely matches the measured data in trend and magnitude.

Although the radial NO profile at 150 mm shows acceptable agreement for the model, the predicted effluent NO concentration was well above the equilibrium value. The suspected reason for this result is the failure of specific kinetic assumptions used in deriving the rate expressions. The assumption is made that in the early regions of the reactor, the concentration of NO is small; thus, the reverse rates (decay of NO back to O , N , O_2 and N_2) in the Zeldovich mechanism are negligible. In the upcoming quarter, both the forward and the reverse rates will be employed in the final rate equation, thereby providing for NO_x formation to be bounded by the equilibrium values.

Fuel NO Mechanisms - Some success has been demonstrated with the NO_x submodel of PCGC-2 for predicting fuel NO formation and destruction in bituminous coal flames over diverse conditions. However, NO_x predictions for low-rank coals have often lacked good quantitative agreement. One explanation for this has been suggested to be the exclusion of NH_3 as a species in the currently employed global model. Experimental studies have suggested that NH_3

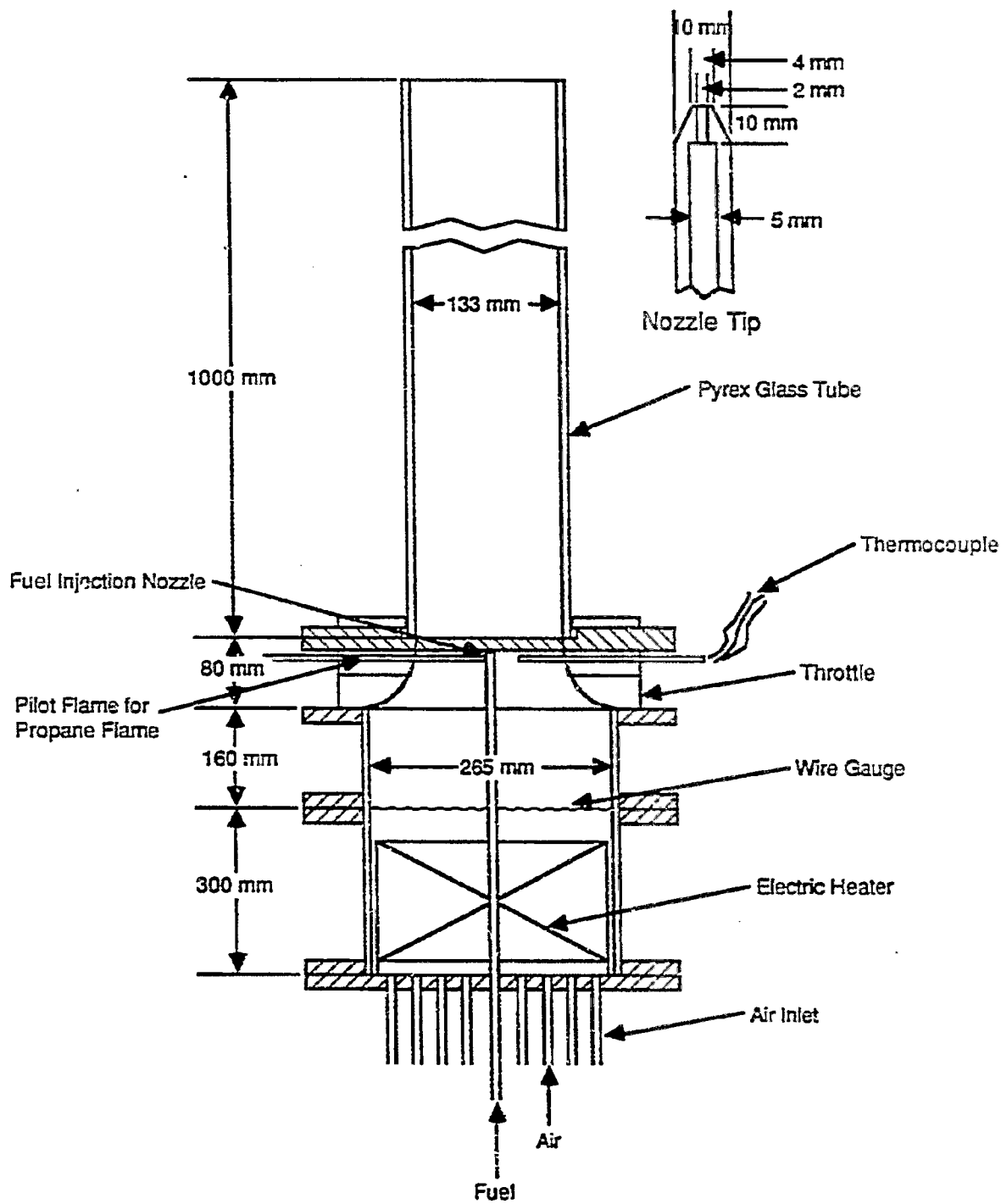


Figure II.G-2. Turbulent jet, propane/air reactor schematic (Takagi, et al., 1981).

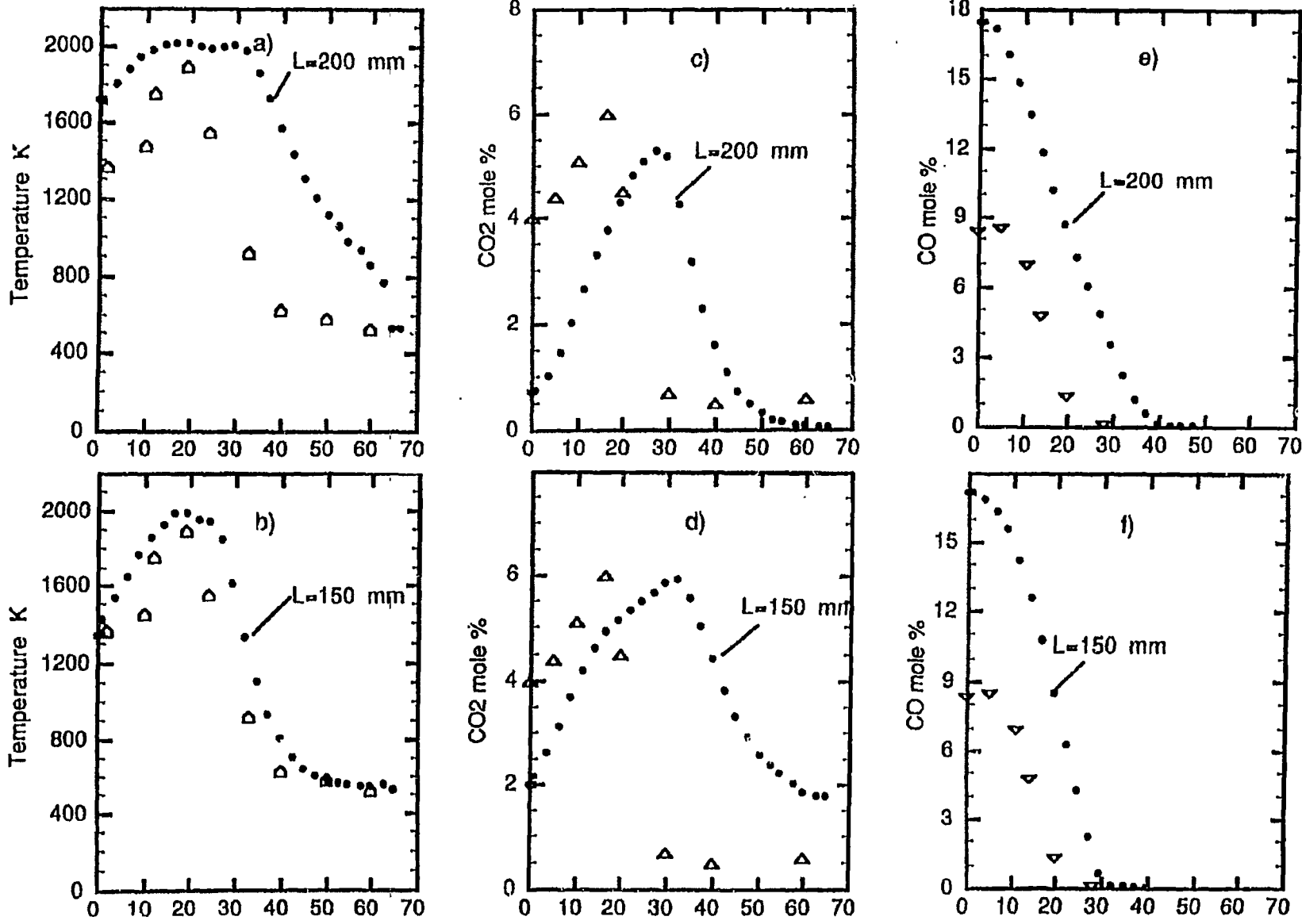


Figure II.G-3. Propane/air combustion case (• - predictions, open symbols - experimental data at L = 200 mm).

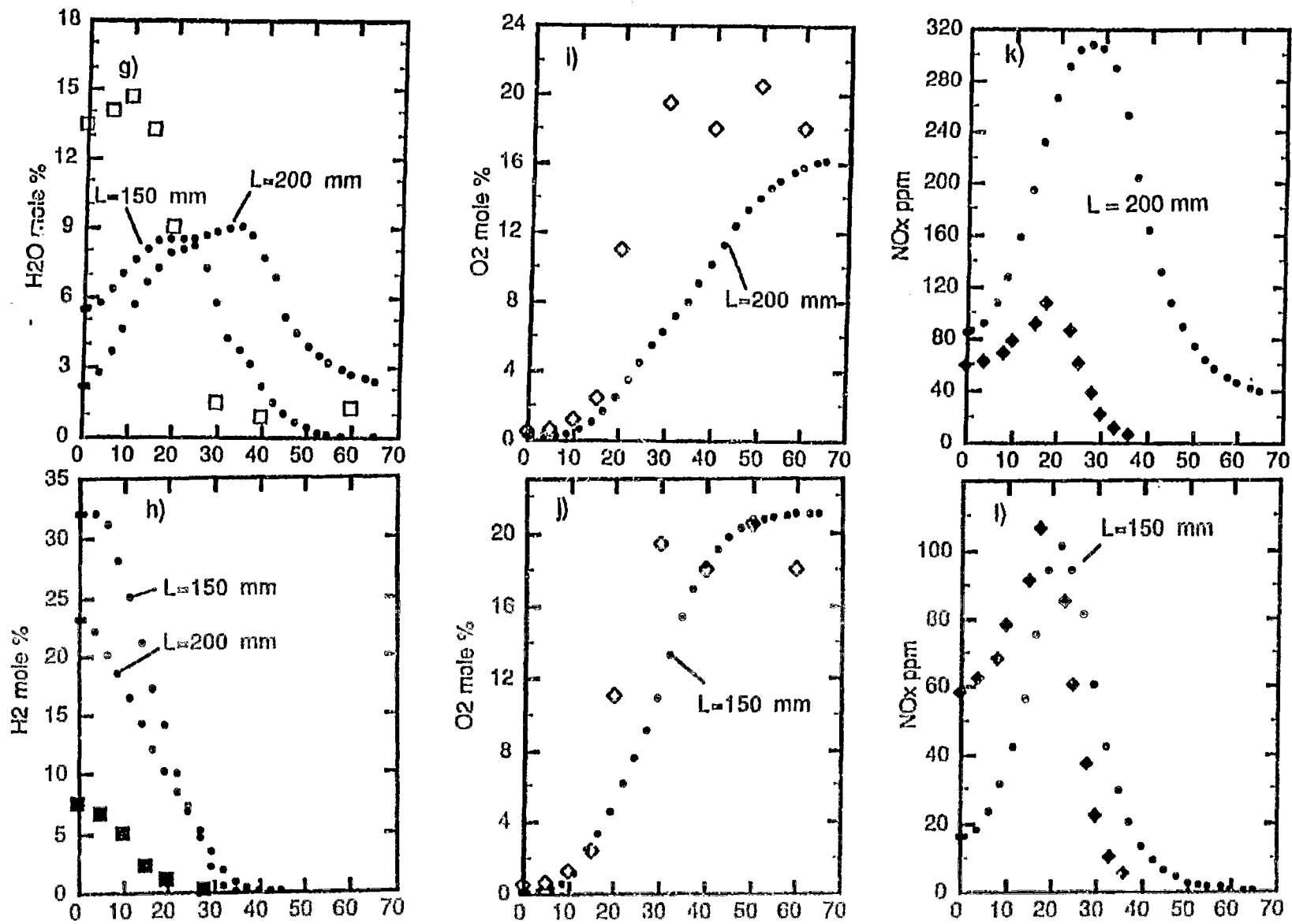


Figure II.G-3. continued.

concentrations are significantly higher than HCN concentrations in subbituminous and lignite coal flames. A review of on-going NO_x work has been completed with the purpose of identifying possible alternative global fuel-NO mechanisms which include NH₃ in the rate equations. From the many fuel NO studies reviewed, two simplified mechanisms have emerged as potential options.

Fenimore (1971, 1972, 1976, and 1979), measured traverses of HCN, NH₃, and NO throughout the burnt gas of very rich, gaseous flames and postulated decay reactions for each species. According to this mechanism, HCN is destroyed through:



and NO is destroyed with N₂ being formed by the reaction:



Fenimore estimated the radical concentrations assuming ammonium radicals are equilibrated by the reaction,



with global equilibrium taken for hydroxide concentrations,



A nitrogen balance, assuming NH₂ is present at concentrations much less than NH₃, yields the following destruction rates for HCN, and NO:

$$\frac{d(Y_{\text{NH}_3} - Y_{\text{NO}})}{dt} = k_1 \frac{Y_{\text{HCN}} Y_{\text{H}_2\text{O}}}{Y_{\text{H}_2}^{\frac{1}{2}}} \quad (\text{II.G-5})$$

$$\frac{-d(Y_{\text{NO}})}{dt} = k_2 \frac{Y_{\text{NO}} Y_{\text{NH}_3}}{Y_{\text{H}_2}^{\frac{1}{2}}} \quad (\text{II.G-6})$$

These global rates apply specifically to the decay of nitrogenous species but do not account for the formation of either NO or HCN. Investigators have applied the Fenimore reactions to coal systems to determine better rate parameters (Glass and Wendt, 1982; Dannecker and Wendt, 1984; Bose and Wendt, 1987; and Bose et al., 1988). In a study of fuel-rich combustion of pulverized coal, Dannecker and Wendt (1984) determined that although there is some variation from coal to coal, their data support the hypothesis that N₂ and NH₃ formation and NO destruction follow the Fenimore mechanism. The destruction of NO appeared to be approximately first order which was consistent with Fenimore's mechanism only if NH₂ is constant.

Bose and coworkers (Bose and Wendt, 1987; Bose et al., 1988) have attempted to further analyze the governing mechanism of NO and other nitrogenous species in the post-flame region of fuel-rich, pulverized coal flames using time-resolved data for a variety of coal types. Their work focused exclusively on the second zone of a staged combustor (where fuel-rich conditions prevail for long time scales (1-2 s) in the post-flame region) before final air addition. They attempted to correlate the decay of nitrogen species for eight types of both low- and high-rank coals, combining the Fenimore decay expression and the reactions supported by Morley, Haynes and Branch, which together yield the expression:

$$\frac{1}{[NO]} \frac{d[NO]}{dt} = [NH_3] \left(\frac{k_1}{[H_2]^{\frac{1}{2}}} + \frac{k_2}{[H_2]} + \frac{k_3}{[H_2]^{\frac{3}{2}}} \right) \quad (II.G-7)$$

The power of [H₂] corresponds to (3-i)/2 with 0 ≤ i ≤ 2 where i is defined by the NO destruction reaction:



The Fenimore mechanism is a special case of Equation II.G-3 when k₂=k₃=0.0 (i.e. i=2 only).

Except under very fuel-rich conditions (stoichiometric ratio < 0.5) Bose et al. (1988) found that both the Fenimore mechanism and the extended mechanism (including terms where i = 0,1,2) could not accurately predict the decay of NO assuming [OH] is globally equilibrated. An empirical correlation was developed

from the experimental gas phase data and rate coefficients to estimate the non-equilibrium [OH] concentrations in the post flame region:

$$Y_{OH} = Y_{OH}(\text{equil}) * 1.8266 \times 10^{-4} \exp(14651/T) \quad (\text{II.G-9})$$

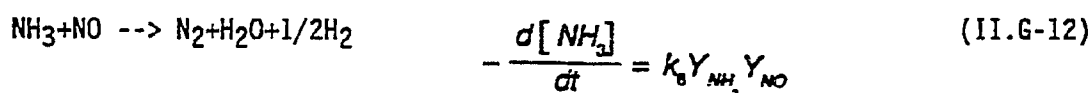
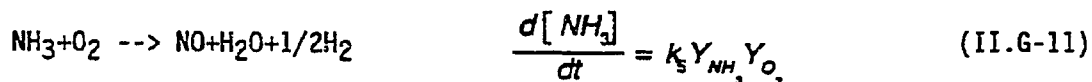
This correlation was then used to predict radical [OH] in the destruction rates. The agreement among experimental and predicted profiles was improved considerably.

Using experimental NH_3 data and measured rates for $d \log[\text{NO}]/dt$, Bose et al. (1988) then derived the least squares fit:

$$\frac{1}{Y_{\text{NH}_3}} \frac{d \log_{10} Y_{\text{NO}}}{dt} \times 10^{-3} = 1.92 \times 10^4 \exp\left(\frac{-11400}{T}\right) \quad (\text{II.G-10})$$

which reasonably represented NO destruction in the post-flame region at stoichiometric ratios of 0.8 and 0.6 for most coal types in their study. This correlation can be considered for predicting NO destruction rates for all coals if NH_3 concentrations can be correctly estimated.

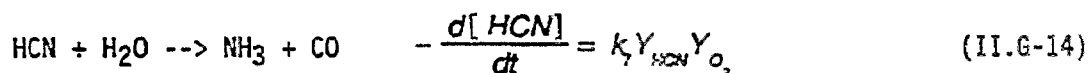
Although variations of Fenimore kinetics may be useful for predicting the decay of NH_3 and NO in the post-flame region, it is also desirable to predict the formation rates of these species. Mitchell and Tarbell (1982) have exploited ideal reactor data to obtain global rates correlating NH_3 , HCN, NO, and N_2 as active centers. They justify the use of NH_3 as the only NH_i radical used in the global scheme based on the suggestion of Haynes (1977) that the NH_i ($i=0-4$) pool is internally equilibrated. The extensive data of Muzio et al. (1977) covering a broad range of temperature and ammonium-NO stoichiometries in CH_4 /excess-air flames in a plug-flow reactor were correlated to rate equations having the global form:



Thus the global reaction describing NO formation is of the type:



The decay of HCN was presumed to be initiated by the attack of an oxidizing agent. Thus, the conversion of HCN to the NH_i center was correlated with the form:



These global expressions are being further investigated to determine their suitability as an alternative fuel-NO mechanism in the NO_x submodel.

Component 2 - Sorbent Particle Chemistry

This subtask component is aimed at developing a sorbent particle submodel for incorporation into PCGC-2. The submodel will include both calcination chemistry and reactions with the gas phase. The submodel will be an extension of independent work being performed by Pershing and coworkers at The University of Utah, where a sorbent chemistry submodel for fuel-lean conditions is being developed and incorporated into PCGC-2. To facilitate the incorporation of the Utah submodel into PCGC-2, the code is currently being tested on the Sun-4 computer. As soon as the code is tested, it will be sent to The University of Utah, where the initial version of the sorbent chemistry submodel will be incorporated.

Component 3 - SO_x Formation

This subtask component will model the gas-phase reactions that generate the sulfur species for input to the sorbent capture model developed under Component 2 of this subtask. A review of the literature is being made to identify recent work related to sulfur pollutants. Objectives include: 1) identifying the steps and kinetics in the SO_x formation process, 2) isolating the most important or rate-determining steps, 3) identifying the dominant products or stable species in combustion gases, 4) determining whether an equilibrium approach is

acceptable, 5) gaining a comprehensive understanding of the effect of reactor parameters and operating conditions on the sulfur species, and 6) identifying important SO_x/NO_x interactions.

SO_x Submodel Development - A review of recent published literature regarding sulfur pyrolysis from coal and gas phase conversion to sulfur species has been completed. The following aspects must be adequately described in order for the predictive method to have any degree of reliability. Each of these aspects involve complex mechanisms which are not completely certain.

1. The physical and chemical transformation of sulfur constituents in the coal during pyrolysis (i.e., rank dependence, temperature programming, extent of sulfur release, and phase conditions - tar, gas, ash, or gas).
2. Chemical conversion of the devolatilized sulfur species to stable species via homogeneous and heterogeneous reactions, i.e. whether the conversion process is kinetically limited or whether a fast-chemistry (equilibrium) assumption applies.
3. Secondary interactions including NO_x/SO_x and alkali metal reactions, capture of sulfur species by injected sorbents, and sulfur deposition in the ash. Until recently, very few correlations between the sulfur in coal and its distribution in the products and evolution rates have been available. Separate investigations are in progress to correlate the influence of coal type (i.e., total coal-bound sulfur and/or sulfur forms) with the distribution among solid (char) liquid (tar) and gaseous phases during devolatilization (Khan, 1988; Mohammad, 1988; Oh et al., 1988). The yields of these phases and the distribution of early volatiles between H_2S and COS have been measured and correlated with various models. These correlations are encouraging for resolving the first aspect listed above.

The chemistry of sulfur in flames has received considerable attention; for example, Cullis and Mulcahy (1972) reviewed over 400 papers of related works published by the early 1970's. In more recent years, some of the key studies of

fuel-sulfur reactions have been made by Kramlich et al. (1981), Solomon (1977), Highsmith et al. (1985), Zaugg (1984), and Nichols (1985). The latter four studies pertained to the evolution and formation of sulfur pollutants during coal combustion and gasification. Zaugg presents a comprehensive review of sulfur reaction mechanisms, outlining the preferred pathway for the oxidation of the sulfur intermediates under fuel-lean and fuel-rich conditions. He also discusses possible interactions between sulfur and nitrogen as well as the capture of SO₂ by alkaline metals. The simplified reaction scheme shown in Figure II.G-4 is suggested for formulation of a sulfur pollutant model.

The empirical rates currently emerging in the literature will be useful for predicting the release of coal-bound sulfur. Further simplification of this mechanism can be made assuming equilibrium conditions exist for the distribution of gaseous sulfur species. If the equilibrium assumption fails to acceptably predict the observed SO₂, H₂S, and COS concentrations, then a well-designed global mechanism should be developed and employed. Zaugg discusses the feasibility of describing the reaction paths shown in Figure II.G-4 and suggests some additional simplifications for arriving at a tractable global kinetic model.

Neither the necessity nor the feasibility a detailed kinetic model have yet been determined. These questions will be addressed in the next quarter.

Plans

Plans for the next quarter include a continued effort to develop the revised NO_x submodel. A thermal NO rate expression, which includes the reverse rates of the three-step Zeldovich mechanism, will be tested. Additional data will be sought to further the model evaluation. Consideration will also be given to testing an alternative fuel-NO mechanism in the model to improve predictions for low-rank coal gasification. Development of the SO_x submodel will continue, beginning with an examination of an equilibrium approach to predict the gas phase chemistry.

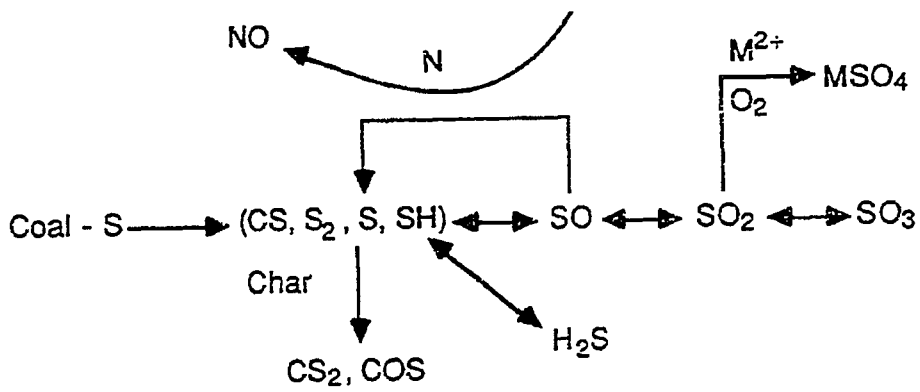


Figure II.G-4. Simplified SO_x mechanism (Zaugg, 1984).

II.H. SUBTASK 2.H. - SO_x/NO_x SUBMODEL EVALUATION

Senior Investigator - Paul O. Hedman
Brigham Young University
Provo, UT 84602
(801) 378-6238

Student Research Assistants - Aaron Huber, David Braithwaite,
Laren Huntsman, and Gregg Shipp

Objectives

The objectives of this subtask are 1) to obtain detailed turbulence measurements for radial crossjet injection of sorbent particles in a cold-flow facility designed to replicate the geometry of a 2-D combustor/gasifier, 2) to obtain concentration profile data for sulfur and nitrogen pollutant species from laboratory-scale, coal reaction tests at atmospheric and elevated pressure with and without sorbents, and 3) to investigate the effect of pressure on the effectiveness of sorbent injection in capturing sulfur pollutants.

Accomplishments

This subtask is being carried out under three subtask components: 1) a cold-flow investigation of sorbent-mixing fluid mechanics, 2) modifications of the laboratory-scale reactor to accommodate sorbent particle injection, and 3) space-resolved sulfur and nitrogen pollutant measurements in the laboratory-scale reactor.

Component 1 - Sorbent Mixing Fluid Mechanics

The BYU cold-flow facility is being used to simulate the flows that exist in the entrained-flow gasifier when sorbent is injected in a flow that is perpendicular to the main gasifier flow. Previous investigators (see Webb and Hedman 1982; Jones et al., 1984; and Lindsay, et al., 1986) have used the BYU cold-flow facility to simulate the flows that exist in one of the BYU coal combustors and the BYU entrained-flow gasifier. The existing cold-flow facility has been modified to include crossflow jets for sorbent injection. Also, the flow chamber design was changed from previous studies. The new flow chamber has

been made of transparent plastic to simplify making LDA measurements and to enable qualitative flow visualization with smoke.

Summary of Related Literature - A review of the literature related to the mixing of turbulent jets in crossflow continued during the period. Ferrell et al. (1985) investigated crossflow injection into a swirling crossflow simulating a gas turbine combustion chamber. Flow visualization with smoke, bubbles and a spark technique were used to highlight the flow patterns for the injected jets. Gross characterization of the flowfield was done for a range of jet-to-cross flow velocity ratios.

Lateral jet injection in an isothermal combustor was investigated by Busnaina (1987) using a three-dimensional computer model. Predictions of the time-mean flowfield for several jet-to-crossflow velocity ratios was presented. Agreement between the computer predictions and flow visualization results were good. However, Busnaina (1987) concludes that a better turbulence model is needed to fully describe the complicated flow situation associated with jets in crossflow.

Facility Modifications - The BYU cold-flow facility has been modified to simulate the geometry of an entrained-flow coal gasifier/combustor, with radial crossflow injection to simulate the injection of sorbent particles.

Preliminary tests were done in the facility using tracer gas injection, and smoke injection for flow visualization. The preliminary tests indicated the presence of a strong recirculation zone at the inlet to the mixing chamber which dominated the flow patterns of the crossflow jets. This recirculation zone was also observed by previous investigators using the cold-flow facility (see Lindsay, 1986). A flow straightener was designed, fabricated and installed in the facility so that the flowfield would better represent a fully developed turbulent flow in a cylindrical reactor.

Figure II.H-1 shows a schematic of the flow straightener design. The flow straightener consists of a thin aluminum plate with six large holes at its circumference. The flow impinges on the center of this plate, and is diverted

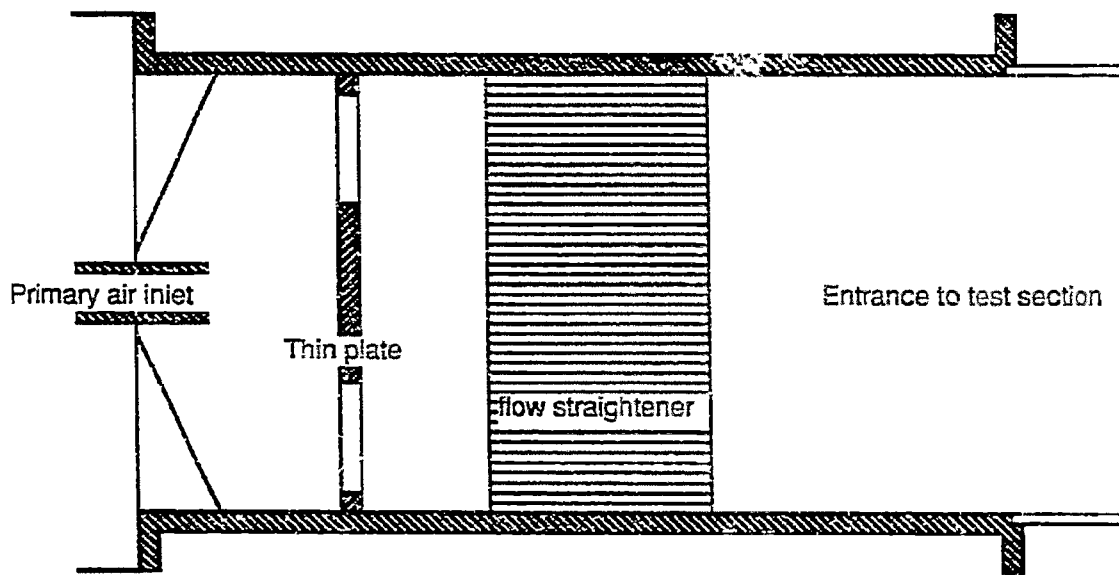


Figure II.H-1. Schematic of entrance to test section of cold-flow facility designed to simulate flow patterns of BYU gasifier.

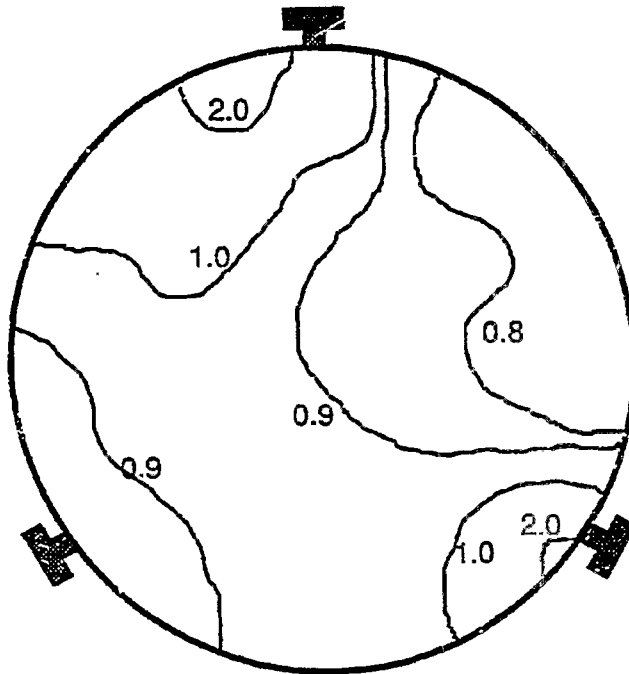
by the holes into a plenum chamber just ahead of a thick aluminum block. The 5-cm-thick slab of aluminum has had several hundred small holes drilled through it in the axial direction. This flow straightener has been demonstrated to effectively straighten the flow and remove the artificial recirculation zones introduced at the inlet to the mixing chamber.

Several tests using CO₂ tracer gas were performed with the flow straightener in various longitudinal positions in relation to the crossflow jets to insure that the flow leaving the flow straightener was uniform. Tracer gas tests showed significant distortion in the mixing patterns of the crossflow jets when the flow straightener was not in place. Figure II.H-2 compares mixing of the crossflow jets both with and without the flow straightener in place. Contours of trace gas mass fraction normalized by the well-mixed mass fraction are shown. Figure II.H-2a shows that the jet profiles were almost indistinguishable without the flow straightener due to the artificial recirculation pattern sweeping the crossflow into other parts of the mixing chamber.

In Figure II.H-2b, the profiles of the crossflow jets being deflected into the main flow are shown. The type of turbulent mixing shown in Figure II.H-2b is in agreement with previous research conducted on deflected turbulent jets. Tests conducted before the flow straightener was installed are not consistent with the results of previous investigations in this area. (see Kamotani and Gerber, 1974; Platten and Keffer, 1971; Pratte and Baines, 1967; and Cetegen et al., 1987.) Without the flow straightener present, the penetration and dispersion of the crossflow jets was dominated by the artificial flow patterns of the recirculation zones that were introduced at the chamber inlet.

Tracer Gas Tests - Once the flow straightener modification had been incorporated into the facility and checked out, testing with the tracer gas was initiated. Gas samples were extracted from the flow using a series of probes in a collar. A 45-point Cartesian grid was employed at each axial location tested, with gas samples taken at each point. The gas samples were analyzed on-line using an IR CO₂ analyzer. Tests were conducted at eighteen different flow conditions. Variables included the main flow Reynolds number, number and location of crossflow jets, and jet-to-main flow momentum ratio. Samples were

a.) without flow straightener



b.) with flow straightener

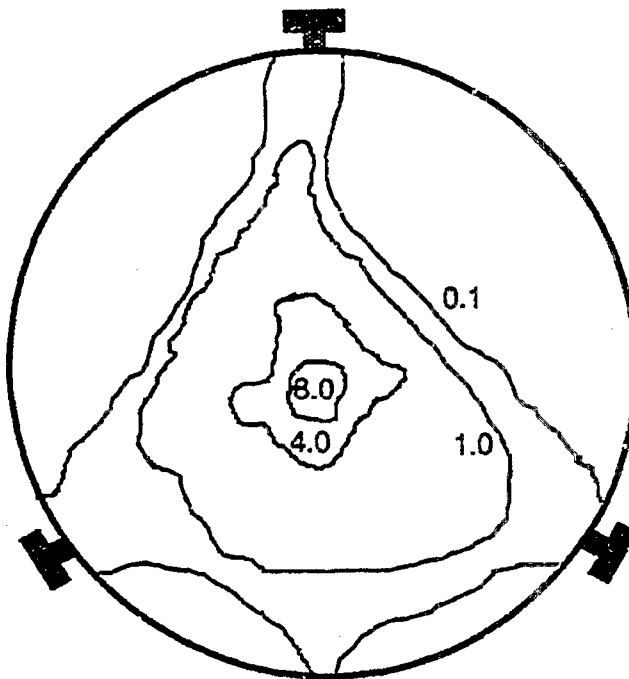


Figure II.H-2. Contours of trace gas mass fraction in the cold-flow test section normalized by the well-mixed mass fraction.

obtained for each case at four different axial locations, making a total of 72 test runs. Some replicate points were also taken to check the reproducibility of the test program.

Figure II.H-3 shows example tracer gas mass fraction contours for one flow case at different downstream axial locations. For the flow case shown, three crossflow jets were employed, the jets being separated by 120 degrees. The dispersion of the crossflow jets can be seen by comparing the contours at the different locations. The data shown were taken at a main flow Reynolds number of 3000. The ratio of the main flow diameter to the jet diameter was approximately 30, and the jet-to-main flow momentum ratio was 64. This translates to a jet-to-main flow velocity ratio of 6.5. At this momentum ratio, the majority of the jet's fluid penetrates to the centerline of the main flow. As the flow moves downstream the jets mix through turbulent diffusion with the main flow.

Component 2 - Laboratory-Scale Reactor Modifications

This subtask component is aimed at modifying the laboratory-scale reactor to accommodate sorbent particle injection. Previous research has shown (Categen et al., 1987; Kamotani and Gerber, 1974) that the two most important criteria in the mixing of crossflow jets are the diameter and momentum flux ratios of the jet-to-main flow. The effect of both criteria will be investigated in these experiments. The lower limit of the sorbent/sulfur ratio will be determined by the amount of sorbent which can be entrained in a given amount of gas while maintaining an adequate sorbent/sulfur ratio, and the upper limit will be determined by the amount of gas and sorbent flow which would overly dilute the gasifier effluent.

Facility Modifications and Maintenance - During the reporting period, the research team continued to work on maintenance and repair of the existing facilities while designing and manufacturing the necessary new facility components. The entire gasifier was recast with new refractory, permitting the installation of high temperature thermocouples in the flame zone of the gasifier. This modification accepted the modified injector section and permitted the installation of the reactor section which contains two sight

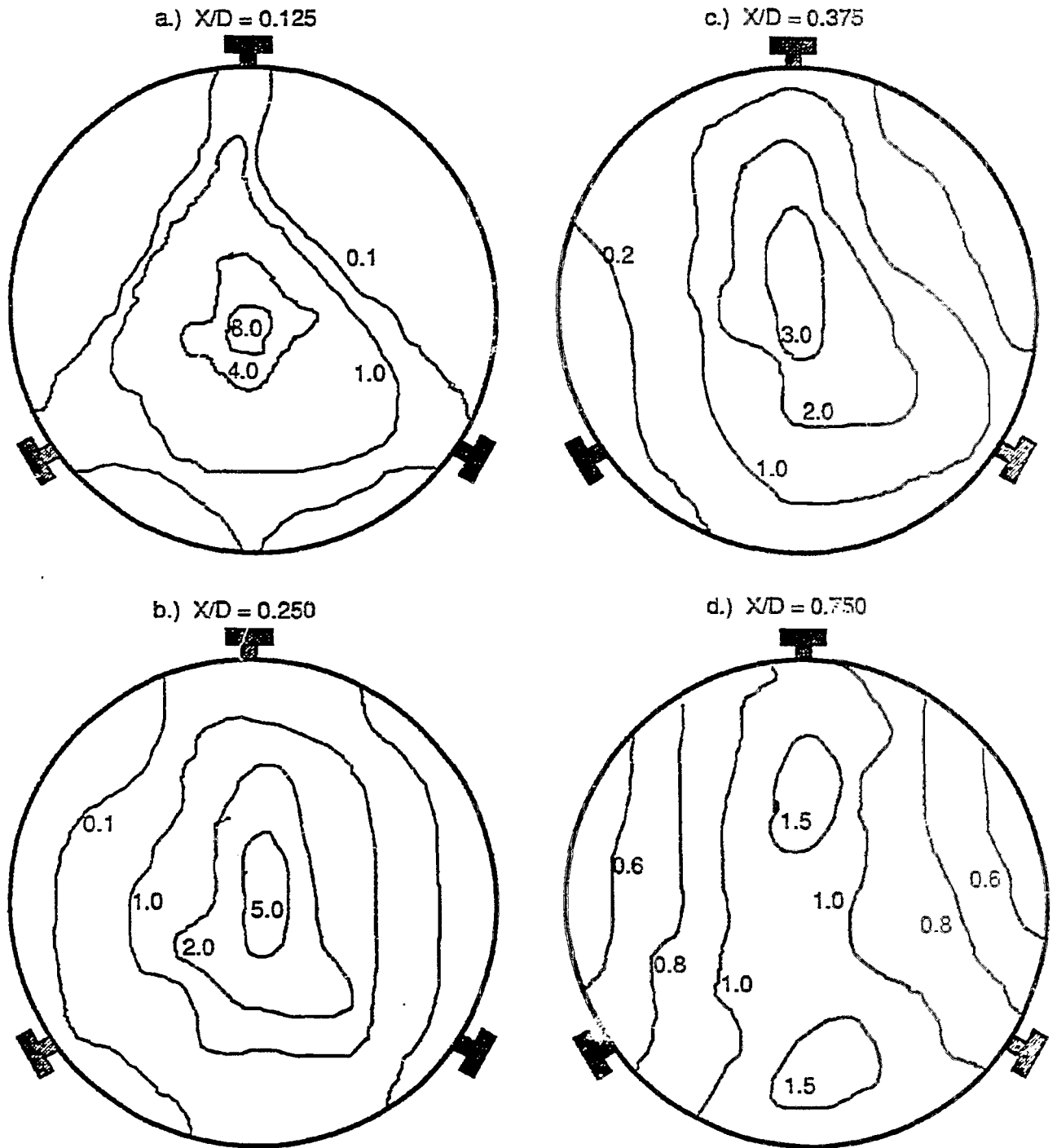


Figure II.H-3. Contours of normalized mass fraction with flow straightener.

window ports spaced 180 degrees apart, and eliminating any interference from sulfur captured by the old slag layer on the results of the current test program.

The pressurized sorbent feeder was installed and work was performed on calibrating the flow of sorbent from the three feed lines. The flash tank was installed and has been used during the past four operations of the gasifier. The coal feed system, shown in Figure II.H-4, has the load cell hooked up to an amplifier and strip chart recorder so that the feed rate in kilograms per hour (kg/hr) can be determined. However, the recorder and amplifier were not responsive enough for our desired range of feed rates, so the resistors in the amplifier were replaced, and a voltage divider was constructed. These changes resulted in the instrumentation responding to the feed rate as required.

Several checkout tests have been conducted with these new facility additions and modifications. Updates and revisions of the procedures used in operating the gasifier facility have been made and will continue to change as new conditions are encountered.

New Sample Collection System - During the past period, a test was conducted where pulverized limestone sorbent was mixed with the coal (3-to-1 Ca/S ratio) and fed through the coal feed system to the gasifier. Product samples were taken with the water-quenched probe and sample system. This hot test was performed to determine if there were any major effects of the sorbent on the slag and/or wall insulation. No significant effect of the sorbent on either the slag layer or the wall insulation was observed. It did appear that the sorbent might be lowering the melting point of the slag somewhat, because the region of slag buildup in the reactor was moved to an area where slightly lower temperatures exist.

During this test it was determined that the water-quenched sample probe may not be adequate for the type of samples that are needed. Therefore, a new sample system and probe was designed and installed. Instead of the water-quenched probe, a water-cooled, helium-quenched probe was built and installed. If this probe works, it will eliminate the problem of interaction in the sample water between the sorbent and sulfur species.

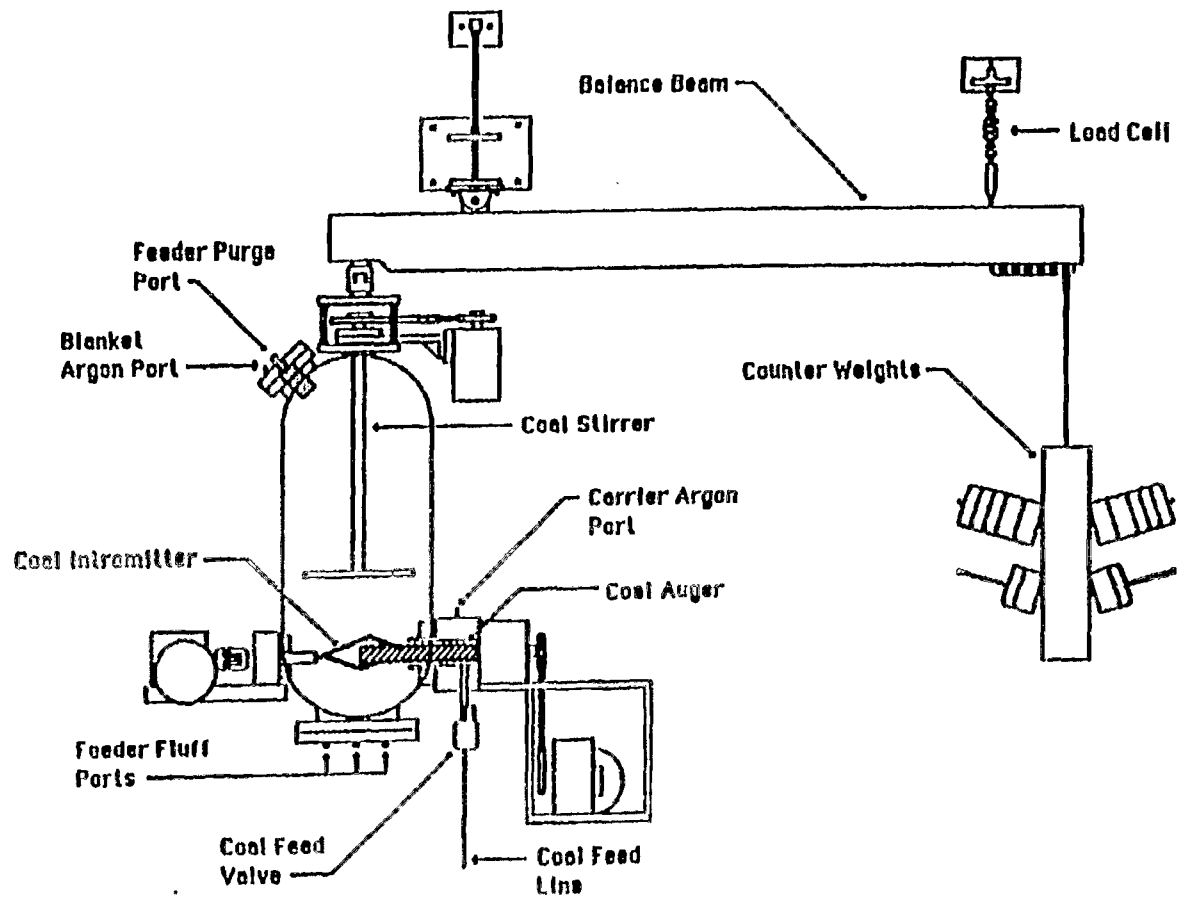


Figure II.H-4. Coal feed system for the Brigham Young University entrained coal gasifier.

The new sample system separates the solid and gas phases soon after the probe and results in only a few milliliters of liquid which has been condensed out of the sample in the collection apparatus. Figure II.H-5 shows details of the new probe. Figures II.H-6 and 7 show a schematic of the sample collection system and the high temperature solid phase filter containers.

An additional checkout test was made to investigate the operation of the new sample system. In this test, which was made with a 4-to-1 Ca/S ratio mix of limestone sorbent and Utah coal, some problems occurred, but overall the operation of the sample system was encouraging. Once the sample system is debugged, it is expected to obtain representative samples of dry char.

Also, a probe consisting of a ceramic tube has been inserted into the gasifier to provide samples of the slag during each run. This will help us determine the effect of the slag on the capture of the sulfur species.

Chemical Analysis Procedures - Char samples obtained from the initial gasifier test with the new sample system are being used to refine the analysis methods. The analysis procedure is being modified to obtain a better measurement of the extent of sulfur capture by the limestone and the form of sulfur species. The modifications that are being considered include the use of non-suppressed ion chromatography to measure Ca^{2+} , SO_4^- , S^- , and CO_3^- that exist in the solid phase.

The soluble species will be dissolved in solution and then analyzed with the ion chromatograph. Because sulfur is captured by limestone as CaSO_4 and CaS , these measurements will indicate how much sulfur is captured as well as how much CaCO_3 remains unreacted. In addition to this method, a Leco sulfur analyzer is being used to determine the total sulfur content of the char samples. Comparing this sulfur content with the sulfur content of the parent coal also gives an indication of the amount of sulfur captured.

Coal Preparation. A quantity of Pocahontas No. 3 coal was obtained and the test plan was modified accordingly. The coals and limestone were pulverized in sufficient quantities for the basic test plan. Because of the importance of the

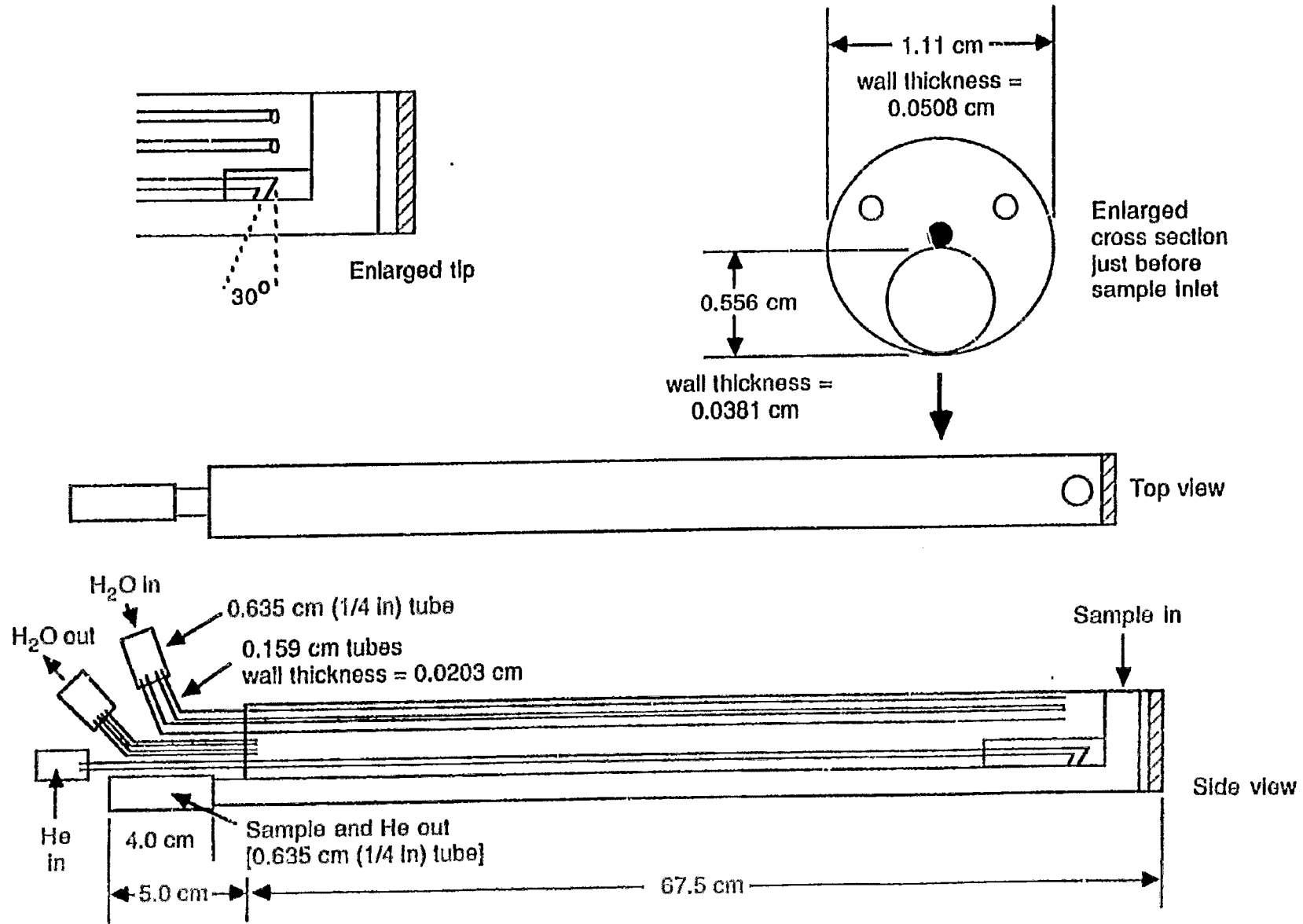


Figure II.H-5. Schematic drawing of the water-cooled, helium-quenched sample probe.

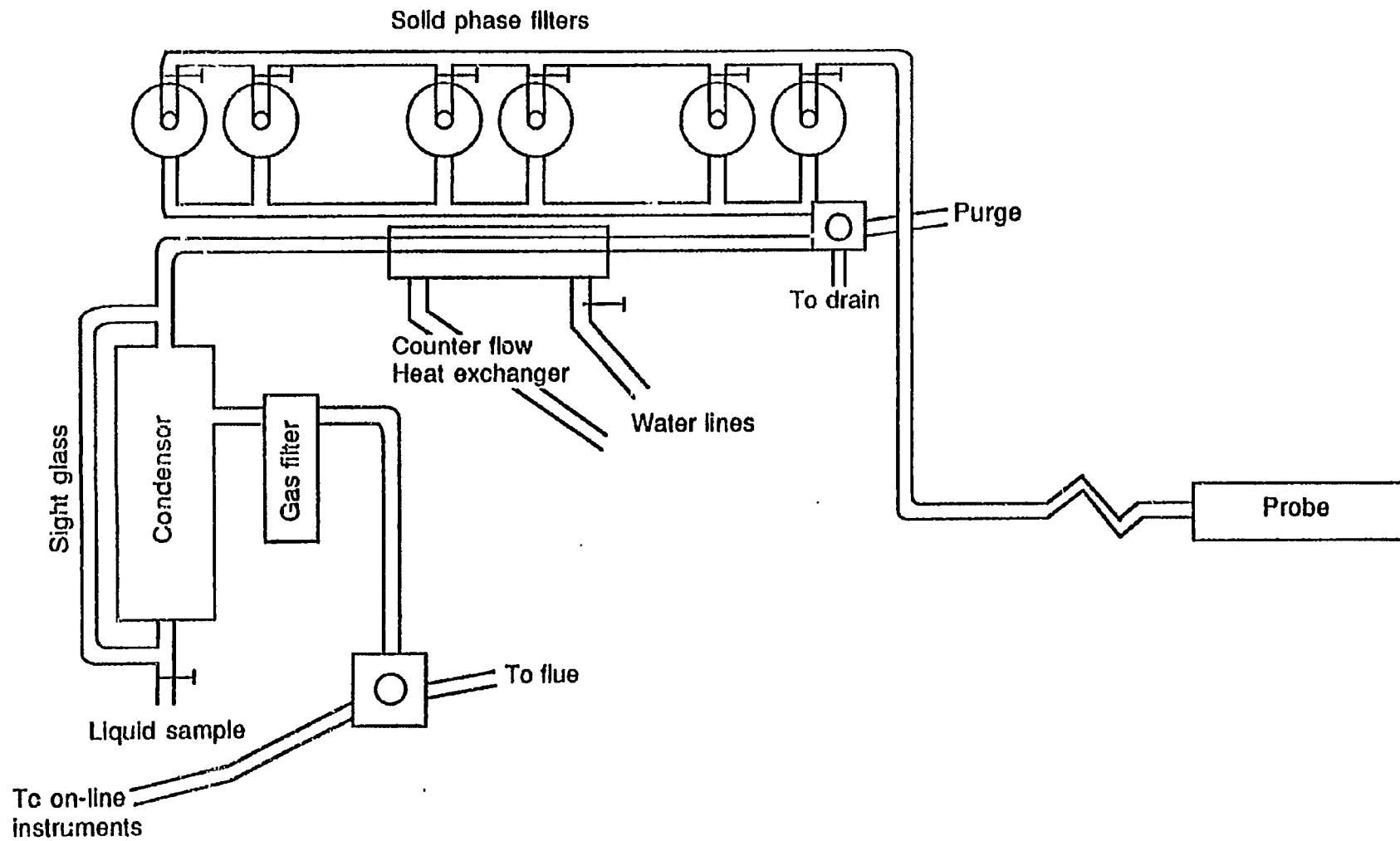


Figure II.H-6. Schematic drawing of the sample collection system.

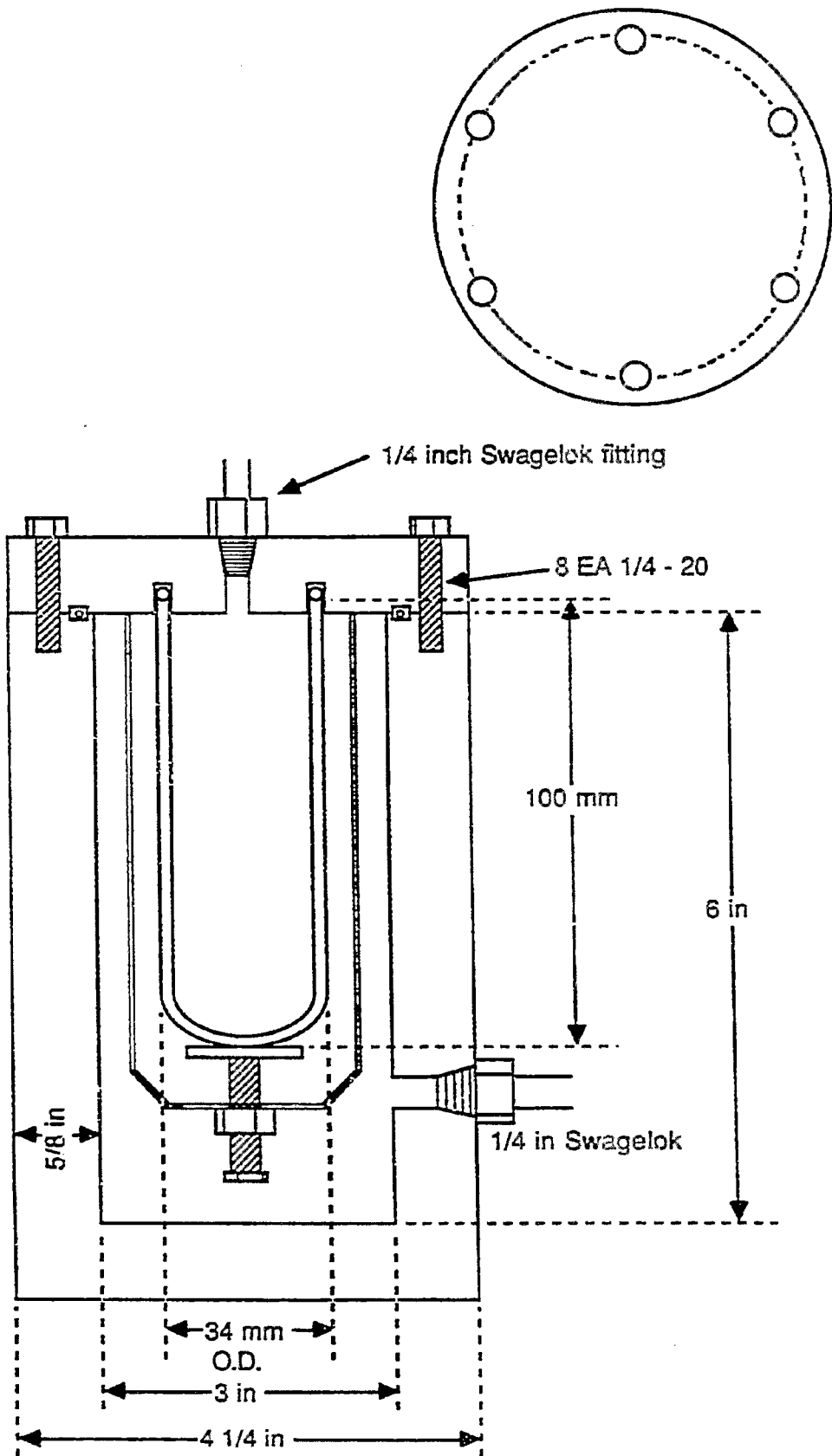


Figure II.H-7. Schematic drawing of the solid sample filter containers.

particle size of limestone on the capture of sulfur shown in previously published research, a mean particle diameter of approximately 1 to 2 microns was desired. Figure II.H-8 is a graph of cumulative fraction of the limestone as a function of the particle diameter. This shows that a 6-micron mean was obtained. The graphs were constructed from reproducible measurements done on a Coulter counter. This is the smallest size limestone particle size that has been obtained using the pulverization equipment available at BYU. Further size reduction with this equipment would require measures well beyond the scope of this study. A check will be made among other investigators to determine possible sources or other methods for obtaining or producing smaller-sized limestone. Otherwise, the 6-micron particle sorbent will be considered for use in these tests. The limestone which was obtained from Henderson, Nevada was also analyzed and found to contain 93.3% calcium carbonate (CaCO_3).

Component 3 - Space-Resolved Sulfur and Nitrogen Pollutant Measurements

This subtask component is aimed at making detailed measurements of sulfur and nitrogen pollutants and char in the laboratory-scale reactor. Work on this subtask will follow the completion of Component 2.

Plans

In the cold-flow study, additional testing will be done to better characterize the flow being investigated, and to make the results useful for validating computer predictions. The few tests remaining using CO_2 tracer gas injection will be completed. Tests using smoke injected in crossflow will be completed to visualize the crossflow jet trajectories. A few tests will also be made using the laser-doppler anemometer facility to determine the velocity profiles at both the main inlet and crossflow jet inlet. LDA testing will also be done downstream from the crossflow injection point, to examine the velocity profiles and turbulence intensity in the mixing zone. The tracer gas, flow visualization and LDA results will be analyzed and compared with results obtained by other researchers.

Work will be continued to maintain and improve the gasifier facility. Checkout tests on the new sample system will be completed. Once the checkout

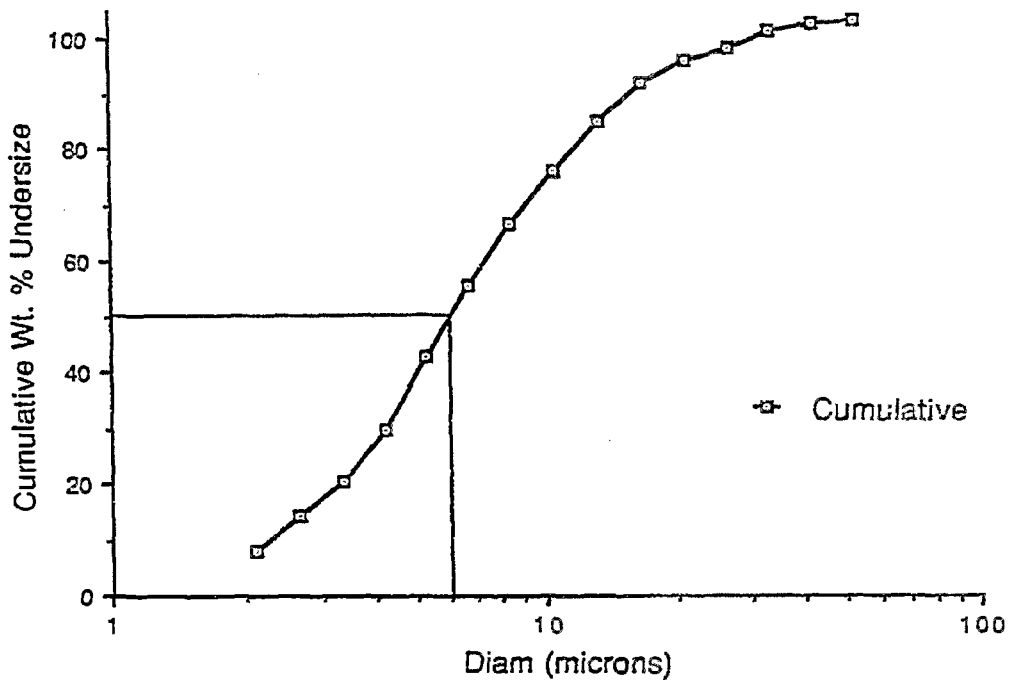


Figure II.H-8. Particle size distribution of limestone obtained from Henderson, Nevada, and pulverized at BYU.

tests are completed, sulfur and nitrogen pollutant measurements with and without sorbent injection will be made. The data reduction program will be used to analyze samples to determine gasification performance and sorbent capture efficiency. Joint tests with AFR will be made later in the summer (scheduled for August 1-5, 1988). AFR will bring their FTIR instrument to BYU, where it will be used to make temperature and species measurements across the flame front in the gasifier.